Annual Report

Hydrospheric Atmospheric Research Center (HyARC)

Nagoya University

2007

Annual Report

Hydrospheric Atmospheric Research Center (HyARC)

2007

NAGOYA
UNIVERSITY

Contents

Progress Reports

Foreword

The Hydrospheric Atmospheric Research Center (HyARC) at Nagoya University was established seven years ago to promote research on the global water cycle, which is one of the primary components of the Earth system. Research on the global water cycle requires strong and extensive collaboration among science and application communities. HyARC functions as an inter-university collaborative system, which may be unique in the world. During the last seven years, the research style of HyARC has become definite, and specific projects/activities have been initiated. The projects/activities include the operation of the International Project Office of the Global Energy and Water Cycle Experiment (GEWEX) Asian Monsoon Experiment (GAME), a subproject under GEWEX, led by Prof. T. Yasunari at HyARC, and the promotion of its follow-on projects. There are three major ongoing projects supported by the Grants-in-Aid for Scientific Research. Projects are being conducted with the support of the Core Research for Evolutional Science and Technology (CREST) of the Japan Science and Technology Corporation (JST), the Global Environment Research Fund, the Innovative Program of Climate Change Projection for the 21st Century, etc. The Ministry of Education, Culture, Sports, Science and Technology, Japan, supported HyARC for constructing a multi-parameter radar system to study water circulation, and funding from an Inter-University Project supported us to initiate a program on climate diagnostics: “Virtual Laboratory for the earth's climate diagnostics.” HyARC has also collaborated with institutions such as the Research Institute for Humanity and Nature (RIHN) and the National Institute of Information and Communication Technology (NICT), and has its own collaborative activities. We have selected four research center projects to be funded by the HyARC budget.

Although funds are limited, the projects are selected based on feasibility, necessity, and collaboration requirements. We have four research center projects and five workshops in this fiscal year. Although the number of permanent staff at HyARC is only 11 (4 professors, 4 associate professors, and 3 assistant professors), many postdoctoral candidates are involved in active research. In addition, we have accepted graduate students in the Department of Environmental Studies. As a part of contributing to the UNESCO International Hydrology Programme (IHP), we have conducted an IHP training course, which is funded by the Japan Trust every Japanese fiscal year. This year, the theme of the IHP training course was “Numerical Prediction of High-Impact Weather Systems.” Nagoya University has undergone a major change toward a flexible management system with an emphasis on accountability. At the same time, research publications and other outreach programs are being encouraged. On the basis of comments by an outside evaluation committee, we would like to propose a new idea of establishing a national and an international grand-scale facility, and a new organization to cater social requirements.

UYEDA Hiroshi
Director
Hydrospheric Atmospheric Research Center

Staff and Organization

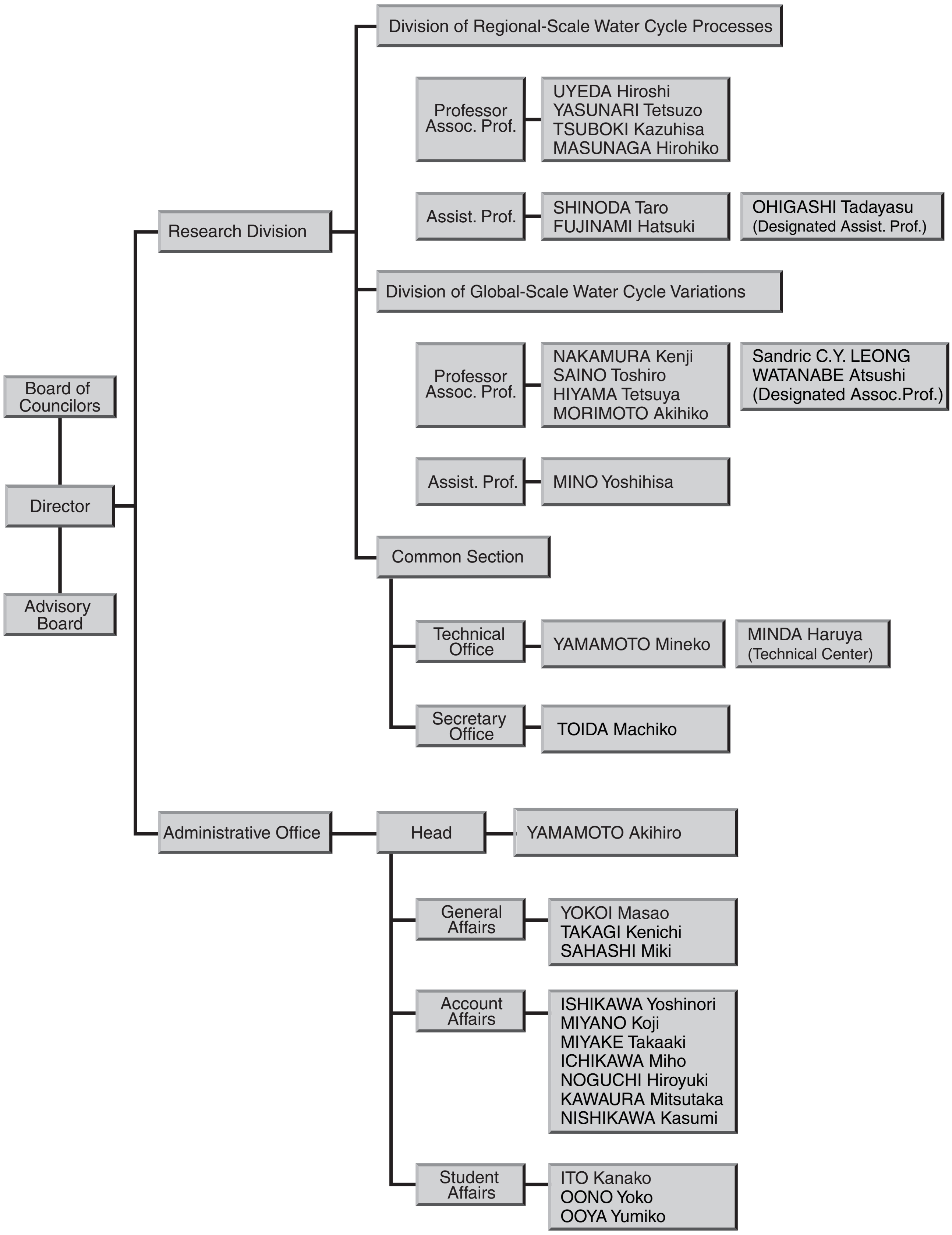

Administration

Board of Councilors

UYEDA Hiroshi: *Director, Prof., Hydrospheric Atmospheric Research Center*

YASUNARI Tetsuzo: *Prof., Hydrospheric Atmospheric Research Center*

NAKAMURA Kenji: *Prof., Hydrospheric Atmospheric Research Center*

SAINO Toshiro: *Prof., Hydrospheric Atmospheric Research Center*

UEMURA Daisuke: *Prof., Graduate School of Science*

TSUJIMOTO Tetsuro: *Prof., Graduate School of Engineering*

HATTORI Shigeaki: *Prof., Graduate School of Bioagricultural Sciences*

KANZAWA Hiroshi: *Prof., Graduate School of Enviromentral Studies*

FUJII Ryoichi: *Prof., Solar-Terrestrial Environment Laboratory*

Advisory Board

- **Members from Nagoya Unisversity**

UYEDA Hiroshi: *Director, Prof., Hydrospheric Atmosphric Research Center*

YASUNARI Tetsuzo: *Prof., Hydrospheric Atmospheric Research Center*

NAKAMURA Kenji: *Prof., Hydrospheric Atmosphric Research Center*

SAINO Toshiro: *Prof., Hydrospheric Atmosphric Research Center*

TSUBOKI Kazuhisa: *Assoc. Prof., Hydrospheric Atmosphric Research Center*

MASUNAGA Hirohiko: *Assoc. Prof., Hydrospheric Atmosphric Research Center*

HIYAMA Tetsuya: *Assoc. Prof., Hydrospheric Atmosphric Research Center*

MORIMOTO Akihiko: *Assoc. Prof., Hydrospheric Atmosphric Research Center*

MIZUTANI Norimi: *Prof., Graduate School of Engineering*

OHTA Takeshi: *Prof., Graduate School of Bioagricultural Sciences*

YAMAGUCHI Yasushi: *Prof., Graduate School of Environment Studies*

MATSUMI Yutaka: *Prof., Solar-Terrestrial Environment Laboratory*

- **Members outside Nagoya University**

FUJIYOSHI Yasushi: *Prof., Institute of Low Temparature Science, Hokkaido University*

HANAWA Kimio: *Prof., Graduate School of Science, Tohoku University*

SUMI Akimasa: *Prof., Integrated Research System for Sustainability Science, The University of Tokyo*

FUKUSHIMA Yoshihiro: *Prof., Research Institute for Humanity and Nature*

YAMANAKA Manabu: *Senior Scientist, Institute of Observational Research for Global Change, Japan Agency for Marine-Earth Science and Technology*

Water circulation studies with new polarimetric radar

A new polarimetric (multi-parameter) radar will be installed at HyARC, Nagoya University, in 2007. This equipment will promote new studies on clouds and precipitation. At the same time, development of many new observational and analytical techniques utializing this polarimetric radar is essential for the promotion of studies on water circulation. Many problems, such as observational methods, analytical routines and data assimilation methods should be developed to utilize observational data from the new radar and amalgamate this with a cloud resolving model.

This research plan aims at promoting new research on water circulation using the new polarimetric radar including existing radar sets. In concrete terms, we will examine and implement observational data of weather phenomena and physical processes of cloud and precipitation systems. We aim to develop new parameters for multi-parameter radar observation and data analysis as well as display methods for the radar data. We will develop software and operational routines for the radar from physical and engineering viewpoints in collaboration with researchers participating in this study project.

Diurnal processes of convection/precipitation systems in the climate system

Diurnal variation in convection and precipitation is a prominent meteorological feature, particularly in the tropics/subtropics and monsoon regions. Energy, water, and momentum exchanges through the diurnal cycle between the earth surface, atmospheric boundary layer, and free atmosphere play a crucial role in global climate models (GCMs) and still cannot reproduce a realistic diurnal cycle in convection/precipitation, including systematic errors in the models.

This research plan aims to clarify the regionality and seasonality of diurnal processes based on TRMM, other remote sensing data, and *in-situ* observational data from rain gauge stations. Cloud resolving models (e.g., CReSS and WRF) and other regional models are also used to elucidate systematic errors in the climate model due to the diurnal cycle. These studies can contribute to the ongoing international project “MAHASRI.” We aim to promote studies on the diurnal process of convection/precipitation in the climate system in Japan.

On December 19, 2007, a domestic workshop, co-hosted by MAHASRI, was held in Hakone. Studies on the diurnal variation of cloud/precipitation systems, including the relationship with terrain, synoptic conditions and intraseasonal variation, were presented. These studies covered areas from the Tibetan Plateau to the Maritime continents. In total, 14 participants presented new scientific results and there was a lively discussion with many participants in the workshop. Future issues on diurnal cycles were also discussed.

Application of stable isotopes of water for evaluation of multi-scale water cycle processes

Stable isotope ratios of water (δD & δ^{18}O) and those anomalies from well-known meteoric water line (d-excess = δD - 8 · δ^{18}O) are good indicators to identify origins of precipitation, river water, groundwater, and the like. Since isotope ratios of water are controlled by kinetic or equilibrium fractionation processes in evaporation or condensation, the ratios are applicable for evaluations of global water cycles as supporting tools for water balance calculation, paleo-climate variations, and basin-scale hydrological studies.

HyARC is conducting mass spectral analyses of stable isotope ratios of water, as one of the HyARC Research Programs. In fiscal 2007, we comprehensively analyzed 2496 water samples upon requested from several domestic researchers.

We applied for a research grant to the Japan Society for the Promotion of Science (JSPS) and were successful in gaining acceptance of our research plan named “Comprehensive Study on Meso-Scale Precipitation System with Use of Stable Isotope Ratios of Water” from fiscal 2005 through 2007. We are also proposing several other methodologies to evaluate multi-scale water cycles in the hydrological processes of evapotranspiration, atmospheric boundary-layer process, cloud development, and precipitation processes. Our current targets are:

- Use of stable isotope ratios of water to understand the mechanism of meso-scale water cycle systems in coordination with other precise meteorological measurements (e.g., multi-band radars, radio-soundings, and rain drop size measurements) together with objective re-analyzed data set, and
- Use of stable isotope ratios of water to model multi-scale water cycle processes.

This research plan also aims to promote studies in isotope hydrology and to link activities from the multi-scale point of view in water cycles among several research groups in Japan. We have conducted an international science symposium named “International Symposium on Water Isotopes and Climates” on December 1–4, 2007 at Nagoya University. A total of 44 participants attended the symposium, and valuable discussions were held on the issues described above.

Observational study of atmosphere and ocean over and around Okinawa Island

The National Institute of Information and Communication Technology (NICT) established an observation center in Okinawa. The center's facilities include a full polarimetric Doppler radar (COBRA), a 400-MHz wind profiler radar, a Doppler sodar, disdrometers, rain gauges, and ocean radars. The collaboration between NICT Okinawa and HyARC began in 2005. Use of the facility was encouraged as one of the inter-university collaboration activities of HyARC.

Since then, in-depth investigations have been continuing. For example, analyses of the polarization radar data, wind profiler data, and ocean radar data. The height characteristics of the bright band in the convective precipitation system were investigated using COBRA data. Diurnal variation of low-level jets in the Baiu season became apparent from the wind profiler radar data. Some results indicated atmosphere–ocean interaction around Okinawa Island; that is, the diurnal variation of the ocean current was shown to have a correlation with the diurnal variation of the surface wind.

Findings on the precipitation systems around Okinawa can be reported in papers. Regarding the ocean radar, the utilization of the data was expanded and the limitations were also clarified. The need for combination with other data, such as satellite data, should be emphasized.

The Okinawa observational data was continuously archived, and the data were opened to the collaborators.

The Innovative Program of Climate Change Projection for the 21st Century (KAKUSHIN Program)

● Cloud Modeling and Typhoon Research

The Innovative Program of Climate Change Projection for the 21st Century (KAKUSHIN Program) is a research program conducted by the Ministry of Education, Culture, Sports, Science, and Technology (MEXT) (for detail, see http://www.kakushin21.jp/). The KAKUSHIN program has started in 2007 and will be performed for 5 years. As a part of the program, a research project named “Cloud modeling and typhoon research” is now performing at HyARC (PI: K. Tsuboki) to develop high-resolution cloud-resolving model and contribute to the accurate projection of future climate by Global models.

Cloud physics is one of the key processes in modeling studies of climate changes, especially those of the global warming. Improvement of the cloud processes is necessary for accurate simulations in global models. The cloud processes are also core processes in simulations of high-impact weather systems such as heavy rainfalls and typhoons. The main objectives of the team “cloud modeling” are the following four topics. (1) Improvements of cloud microphysics of the cloud-resolving model named the “Cloud Resolving Storm Simulator (CReSS)“ will be performed. The dynamic part of the CReSS model will be also improved for accurate and high-speed calculation. (2) Using the CReSS model, cloud parameters of global models will be examined. Satellite observations are used for verification of the cloud modeling. (3) CReSS is coupled with global models interactively for accurate modeling of convective regions. In particular, convective clouds in the tropical region and typhoons are studied by the modeling system. (4) The CReSS model is used for typhoon research (Fig.1). This aims to contribute to verifications of typhoon simulations of global models, and to accurate and quantitative evaluations of typhoon impacts on the human society in the present and warming climates.

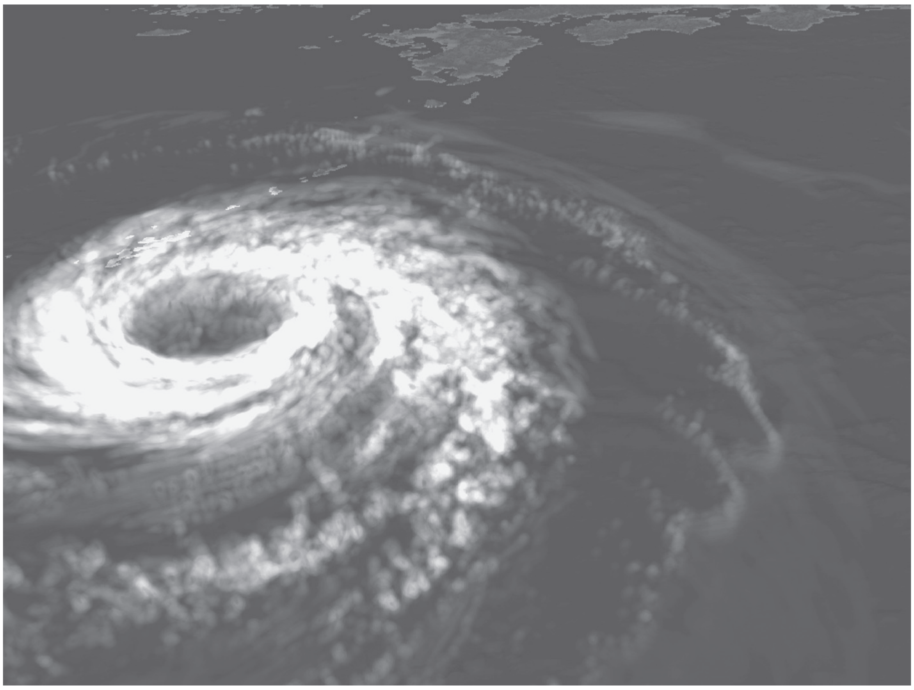

Fig. 1 Three-dimensional cloud display of Typhoon 0418 simulated by the CReSS model with 1 km resolution.

From the SELIS-COE Progarm to the new SELIS (Study Consortium for Earth-Life Interactive System)

● 21st Centruy COE Program "Dynamics of Sun-Earth-Life interactive System" (SELIS-COE) is completed

The SELIS-COE program started from the 2003 fiscal year and 2007. In this program, seamless new research and education system have been improved by strong collaborations through field research and modeling research fields such as Hydrospheric-Atmospheric Science, Earth and Planetary Science, Earth Electromagnetic Physics and Solar Physics. Especially, "Seamless Earth Studies" which aims for understanding of the earth system including the role of biosphere and even human activity has been developed, leading the van of the other universities. Furthermore, the external evaluation committee in May 2007 highly evaluated this program. The necessity of research and educational framework for the earth system studies has also been emphasized in the planning of Global COE program. As part of the educational outcome of the SELIS-COE, a textbook titled "*Atarashii Chikyu-gaku*" co-edited by Dr. S. Watanabe, Dr. T. Hiyama and Prof. T. Yasunari, was published from Nagoya University Press in March 2008. The latter two editors belong to HyARC.

● From the 21th Century SELIS-COE to the SELIS (Study Consortium for Earth-Life Interactive System)

To further develop the pioneering research and educational framework founded by the SELIS-COE, we have established a virtual research institute titled "Study consortium for Earth-Life Interactive System (SELIS)" at the end of March 2008, in collaboration with related colleges and institutions within the university campus, including the Graduate School for Bio-Agricultural Sciences. This institute should play an essential role for further development of tight collaboration between many other institutes and universities within and outside of Japan in the field of the earth system science including the impacts and roles of the biosphere and human activities. The HyARC is expected to play the role as a key institute, including the role of secretariat.

To fully understand and solve the global change issues, such as "the global warming", a new geo-biospheric science needs to be developed, by merging the earth science based on physical and chemical methods and biospheric science based on ecology. Internationally, the studies on the earth system and its variability has been promoted as the "Earth System Science Partnership (ESSP)" under the collaboration with the World Climate Research Programme (WCRP), the International Biosphere-Geosphere Programme (IGBP) and the other programs. The HyARC has promoted research and education related to these international programs and projects since the former Institute of Hydrospheric Sciences (IHAS). Based upon these achievements, the new SELIS needs to be strongly promoted for further development of the collaborative research and education on the earth system science. The role of our HyARC in the new SELIS will become more important than that in the SELIS-COE program.

Solution Oriented Research in Science and Technology (SORST)

● Satellite Monitoring of Ocean Primary Productivity

Ocean is the largest reservoir of water and carbon dioxide on Earth surface, hence the air-sea exchange of water and carbon dioxide plays central role in determining climate system on Earth. The air-sea exchange of heat (water) and carbon dioxide are affected by phytoplankton because they determine optical properties of the near-surface oceans and absorb carbon dioxide by primary productivity. In order to better predict the climate variability, quantitative knowledge of abundance and productivity of phytoplankton on a global scale is required for mechanistic understanding of their regulating processes to improve climate prediction models. Practically, those knowledge and understanding will be attained only by satellites observations, but because of difficulty in obtaining *in situ* data for validation those satellites data are yet to be fully exploited.

To overcome the difficulty, we have been working on to develop an *in situ* monitoring system of ocean primary productivity for validation of satellites primary productivity data. The system composed of an underwater winch system with a profiler buoy equipped with fast repetition rate fluorometer was successfully developed with support of Core Research for Evolutional Science and Technology by Japan Science and Technology Agency. Following this, a continuation project "Satellite Monitoring of Ocean Primary Productivity (SMOPP)" was approved by JST in Solution Oriented Research in Science and Technology Program in 2004. The goal of the SMOPP project is to design an operational monitoring system for ocean primary productivity on a global scale. To attain this goal, we are to conduct a routine operation of the monitoring system and to obtain validated time series satellite data of primary productivity, to be utilized in combination with the other time series satellites data on physical forcing parameters on the ocean surface, for process studies on the response of ocean biology to the atmospheric forcing to the ocean.

Research activities in FY 2007 on the SMOPP project are described separately in the activity report of the Ocean Climate Biology Lab; among them notable achievements are successful long-term operation in Sagami Bay for 100 days, and completion of algorithm to estimate daily-depth integrated gross primary productivity form one single profiling measurement at noon time by the buoy system. As for the Primary Productivity Pofiler, we continued efforts to conduct measurements in various environments as much as possible, such as the northern North Pacific, East China Sea, Sea of Japan, Arabian Sea, North Atlantic, in addition to the Sagami Bay where test mooring of the buoy system is being carried out. The process study using multi-parameter satellites data are being conducted for the Sagami Bay. In order to validate the satellite based process study, cruises of JAMSTEC's Tansei Maru, as well as development of the physical-biogeochemical model, are being continued for observational study on rate processes relating to oxygen metabolism of the Bay.

Division of Regional – Scale Water Cycle Processes

Laboratory of Meteorology

Distribution of precipitation particles in convective cells around Okinawa Island during the Baiu period

In a humid environment such as in Okinawa during the Baiu period, convective cells whose echo-top height was quite low and those in a stratiform rain zone were observed. For clarifying the distributions of precipitation particles in these convective cells, we performed observations on Okinawa Island during the Baiu period using a C-band polarimetric radar and a disdrometer.

We analyzed polarimetric variables and rain drop size distribution (DSD) in convective cells associated with the Baiu frontal rainband on June 10, 2006 using polarimetric radar and disdrometer data. Two convective cells were selected for the analysis. One was embedded in a stratiform rain zone (Fig. 1a) and the other existed in a convective rain zone (Fig. 1b) associated with rainbands. Both convective cells had low echo-top heights (of 30 dBZe) below the height of 6 km, and exhibited intense reflectivity in their convective cores. By analyzing the polarimetric variables, it was determined that a large number of small raindrops contributed to the intense reflectivity below the height of 3.5 km in the former case. This fact was supported by DSD observations, which showed the large contribution of small raindrops (1 to 2 mm in diameter) to the strong rainfall intensity on the ground. Some large raindrops contributed to the intense reflectivity in the latter case. This fact was also supported by DSD observations, which showed the large contribution of large raindrops (exceeding 3 mm in diameter) to the strong rainfall intensity on the ground. From these results, the distribution of precipitation particles in each convective cell was expressed schematically in Fig. 2.

To confirm the generality of this result, 31 convective cells embedded in the stratiform rain zone and 29 cells in the convective rain zone were analyzed using polarimetric variables. A large number of small raindrops contributed to the intense reflectivity in convective cells embedded in the stratiform rain zone, and large raindrops contributed to the reflectivity in the convective rain zone below the height of 3.5 km. These characteristics were the same as those of the two convective cells mentioned above. Thus, we revealed the two types of distributions of precipitation particles in convective cells associated with the Baiu frontal rainband on June 10, 2006; the predominance of small raindrops in the convective cell embedded in the stratiform rain zone, and the existence of large raindrops in the convective rain zone.

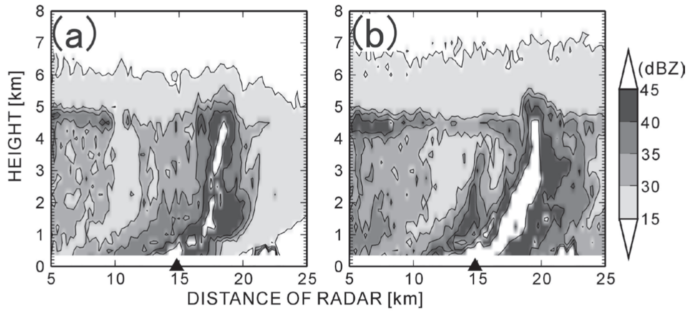

Fig. 1. Vertical distribution of radar reflectivity in RHI of the convective cell embedded in the stratiform rain zone (a), and that in the convective rain zone (b). The symbol ▲ denotes the position of the disdrometer observation site.

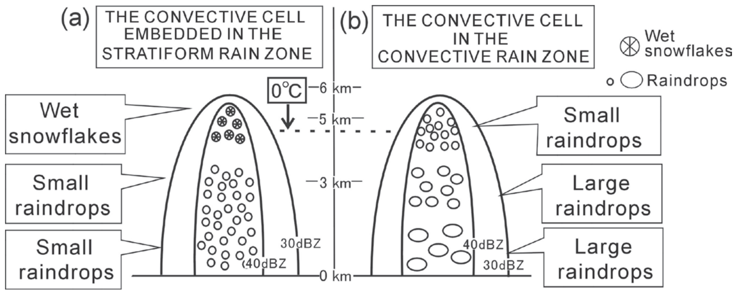

Fig. 2. Schematic distribution of precipitation particles in the convective cell embedded in the stratiform rain zone (a), and that in the convective rain zone (b).

Structure of precipitation cell lines oblique to the Baiu front observed around the Southwest Islands of Japan

This study revealed the structure of “precipitation cell lines (PCLs)” oblique to the Baiu front generated around the Southwest Islands of Japan on June 10, 2006, using data obtained from two X-band Doppler radars located at Shimoji and Tarama Islands.

PCLs appeared every several tens of kilometers in the heavy rainfall area along the Baiu front, extending from west-southwest (WSW) to east-northeast (ENE) for 300 km (Fig. 3). These PCLs consisted of several precipitation cells aligned from south-southwest (SSW) to north-northeast (NNE). The length of the PCLs ranged from 20 to 40 km, and the alignment of the PCLs was parallel to the vertical wind shear between 0.5 and 3 km in altitude. Precipitation cells were generated in the southern part of PCLs, where a large low-level convergence area existed. They moved northeastward corresponding to the horizontal wind velocity at the height of 3 km, and decayed in the northern part of the PCLs, where a large low-level divergence area existed (Fig. 4). The cells in the southern part of the PCLs were in the developing stage in their life-cycle, those in the central part were mature, and those in the northern part were in the decaying stage (Fig. 5).

New cells constructing PCLs were generated at the rear of the pre-existing cells that propagated northeastward. This structure represented the characteristics of the “back-building” line-shaped precipitation systems. However, the downdraft of the pre-existing cell was weak, and the low-level southward flow from the northern cells was not observed by dual-Doppler analyses (Fig. 5). The fact that pre-existing cells did not affected on the generation of new cells should be attributed to the lack of evaporation cooling, due to the high humid field in the lower troposphere around the Baiu front. Further, convectively neutral stratification appeared in the northern part of the PCLs. Therefore, the new cells developed only in the southern part of the PCLs, where a low-level convergence existed along the Baiu front. The length of the PCLs corresponded to the product of the life span and speed of each cell relative to the PCL. Thus, using only observation data, this study revealed that PCLs oblique to the Baiu front were the “back-building” line-shaped precipitation systems that occurred in the high humid field in the lower troposphere.

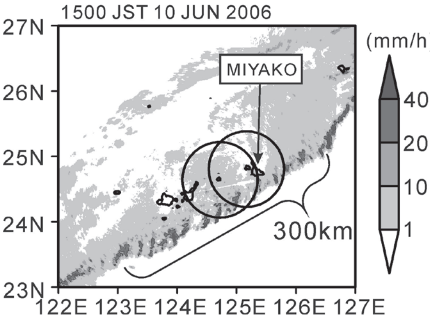

Fig. 3. Rainfall intensity distributions observed by the JMA radar at 1500 JST on June 10, 2006. The ranges of the Doppler radars installed at Shimoji and Tarama Islands are indicated by circles.

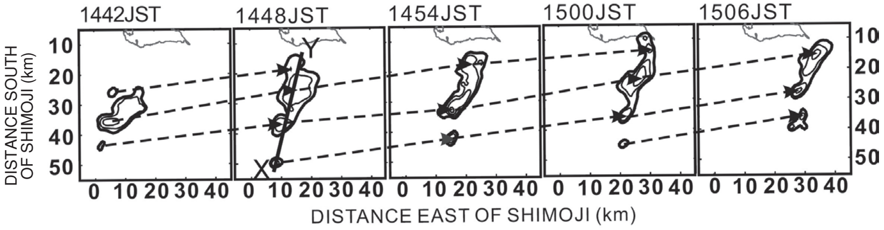

Fig. 4. Reflectivity distributions at the height of 2 km observed by Doppler radars at 6-min intervals from 1442 to 1506 JST on June 10, 2006. Only the precipitation area related to a PCL is shown. The reflectivity is contoured at 2-dBZe intervals from 32 dBZe. The arrows indicate the propagation of each precipitation cell.

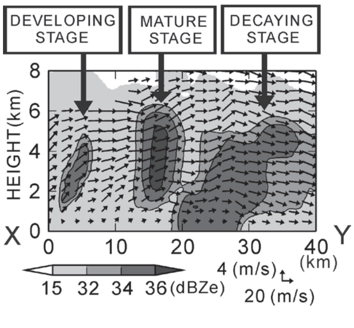

Fig. 5. Vertical cross section of the distribution reflectivity (shades) and horizontal and vertical wind vectors (arrows) at 1448 JST on June 10, 2006 along the X-Y line of Fig. 4.

Simulation Experiments of Supercells and Tatsumaki along Typhoon Rainbands

Tornadoes and waterspouts are a violently rotating air below a convective cloud. They are called "tatsumaki" in Japan. In Japan, 20.5 tornadoes and 4.5 waterspouts occur on average and about 20% of tornadoes occur in association with typhoons.

Even through a typhoon center is located in the far distance, a disaster due to a strong wind is occasionally caused by a "tatsumaki". When Typhoon 0613 (T0613) moved northward off the west of Kyushu, a severe disaster was caused by an intense tatsumaki along the east coast of Kyushu. The tatsumaki occurred when typhoon rainbands moved northward along the east coast. Two simulations with different horizontal resolutions were performed using the Cloud Resolving Storm Simulator (CReSS) Ver.2.2 in the present study. The experiment with a horizontal resolution of 500 m successfully simulated not only the overall structure and movement of T0613 but also a detailed structure of the typhoon rainbands. The other experiment with a resolution of 75 m simulated that a tatsumaki forms in convective clouds. The result shows that the outermost rainband was composed of suprecells which involve a meso-cyclone. Tatsumakis form within the supercells.

A detailed structure of the supercell which produced a tatsumaki was simulated (Fig. 6). The supercell extends the north-south direction with a horizontal length of 20 km. Intense rain occurred in the southern part of the supercell with a very sharp hook-shaped structure at the southernmost part. The tatsumaki is formed in the hook-shaped structure which is indicated by the circle in Fig. 8. A weak rain is present in the northern part of the cell.

A close view of the southern part of the supercell (Fig. 7) shows that the tatsumaki forms inside of the hook. The horizontal scale of the simulated tatsumaki is about 300 m, which is the almost same scale with the observed tatsumaki. The experiment of 75 m resolution successfully simulates the tatsumaki within the supercell. The maximum vorticity of the tatsumaki is 0.9 s^{-1} and pressure perturbation at the center is –27 hPa. The pressure field and the velocity field are in the cyclostrophic balance in a high accuracy. This is a most significant characteristic of the tatsumaki.

The wind velocity around the tatsumaki is very large which resulted in the severe disaster in Nobeoka City. The horizontal wind speed of the simulated tatsumaki is larger than 70 m s^{-1} on the east side of the tatsumaki while it is weak in the west side (Fig. 8). This asymmetry of horizontal wind speed well corresponds to the asymmetry of the damage distribution due to the tatsumaki. The damage is significant on the right-hand side of the pass of the tatsumaki while it is small on the left-hand side with the northward movement of the tatsumaki.

Another simulation experiment with a horizontal resolution of 75 m was performed within a much larger domain using the Earth Simulator. A preliminary result shows many tatsumakis were simulated along the typhoon rainbands. Most tatsumakis form along the northernmost (outermost) rainband. This is consistent with that the outermost rainband is composed of supercells in the experiment of 500 m resolution.

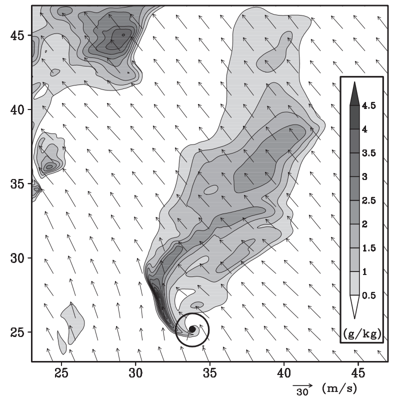

Fig. 6. Supercell at a height of 200 m at 0500 UTC September 17, 2007 obtained form 75 m-resolution simulation. Gray levels are mixing ratio of rain (g kg^{-1}) and arrows are horizontal velocity. The circle indicates the tatsumaki developed in the supercell.

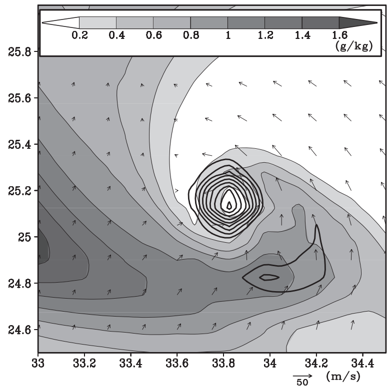

Fig. 7. Enlarged view of the southernmost part of the supercell indicated by the circle in Fig. 1. Gray levels are mixing ratio of rain (g kg^{-1}), contours are vertical voriticity from 0.1 s^{-1} every 0.1 s^{-1}, and arrows are horizontal velocity.

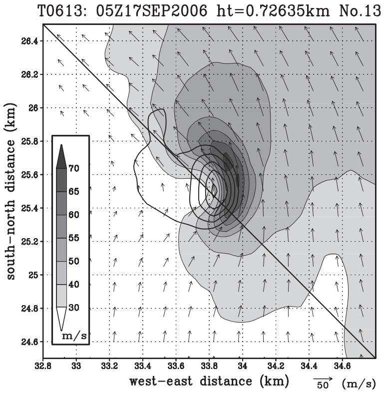

Fig. 8. Horizontal distribution of wind speed (gray levels; m s^{-1}) at a height of 0.73 km at 0500UTC September 17, 2006.

Reproducibility and validation of simulated typhoons using the Cloud Resolving Storm Simulator

Strong winds and heavy rainfall associated with typhoons cause large damage. Highly accurate typhoon forecasts are required to estimate the damage region and non-life insurance premiums. In order to forecast extreme phenomena, it is necessary to use a high-resolution numerical model that resolves spiral rainbands of a typhoon. In this study, we simulated 10 typhoons that caused large damage in Japan, using the Cloud Resolving Storm Simulator (CReSS) and evaluated the results.

Figure 9 shows the observed best track and the results of a 48-h numerical simulation for typhoon Songda (T0418). The simulated track, landfall point on Kyushu Island, and acceleration of the typhoon after landfall, are reproduced well. Although the central pressure error at the initial time is about 20 hPa, it decreased until six hours from the start of the simulation. During the landfall on Kyushu Island, the minimum pressure near the center of the typhoon is 945 hPa and the error is only 1 hPa. The maximum wind speed of over 35 m s^{-1} and the heavy rainfall around Kyusyu are also reproduced well. Thus, the track and intensity of typhoon Songda were successfully simulated using the CReSS.

Next, quantitative validations were performed for all 10 cases. Figure 10 shows a histogram of the rainfall over 20 mm h^{-1}. The CReSS (horizontal grid resolution; dx = 2.5 km) reproduces this heavy rainfall well compared with that reproduced by the Regional Spectral Model (RSM: dx = 20 km). The wind gust is a key parameter for wind disasters. Figure 11 shows a scatter plot of the maximum wind speed observed at meteorological stations and the estimated maximum wind speed calculated from the product of the simulated wind speed and statistical gust ratio in the same grid in the CReSS simulations. The correlation between the simulated and observed wind speeds is very high, 0.83. Therefore, we can consider that the CReSS reproduces the typhoons quite well.

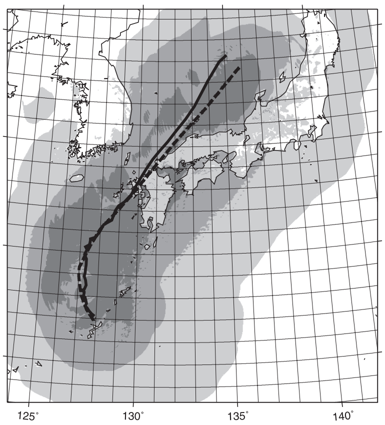

Fig. 9. Best track (broken) and simulated track (solid) of the typhoon Songda. The shaded areas show strong wind regions: 15, 25, and 35 m s^{-1}, respectively.

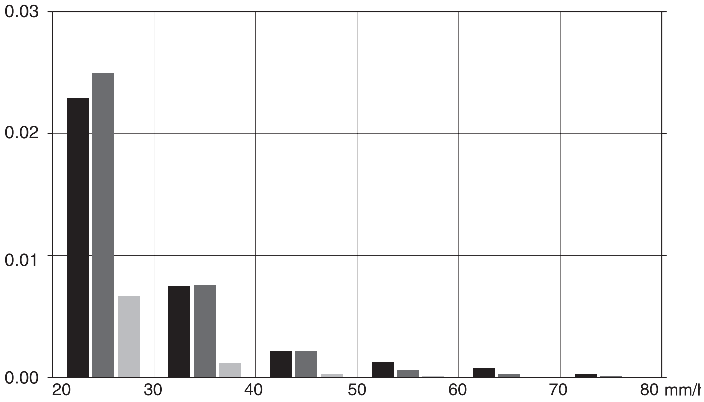

Fig. 10. Histogram of rainfall above 20 mm h^{-1} by observation (black), CReSS (dark grey), and RSM (light grey).

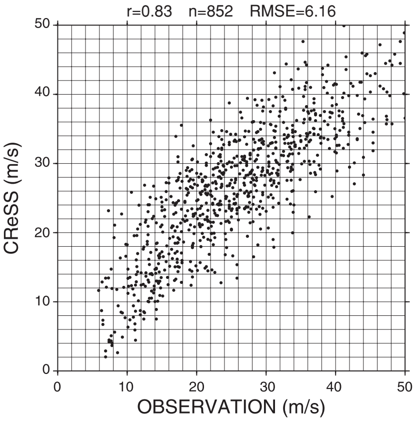

Fig. 11. Scatter plot of the maximum wind speed observed at meteorological stations, and the estimated maximum wind speed calculated from the simulation results.

Probability density function of total water in a grid scale of the general circulation model

There is a large uncertainty about the large-scale condensation processes that prescribe the development of clouds in the general circulation model (GSM). The large-scale condensation processes prescribe the amount of condensation (cloud water/ice amounts) and cloud fraction in each grid, as a result of the prescribed probability density function (PDF) that is assumed for the average value of total water. In this study, we show a PDF for total water using daily simulation results from the Cloud Resolving Strom Simulator (CReSS) for the area around Japan from December 29, 2004 to December 16, 2005. The total number of simulations was 303. The horizontal and vertical grid resolutions of the simulation were 5 and 0.5 km, respectively. Data of every hour from the start of the simulation were used for the PDF analysis. Mixing ratio of total water, which was the sum of that of water vapor, cloud water, rain, cloud ice, snow, and graupel, was averaged for the horizontal scale of about 280 × 280 km^2, which supposed a horizontal grid resolution of T42-GCM. The PDF of total water was calculated in each bin (every $0.1\,\mathrm{g\,kg^{-1}}$) of averaged mixing ratio of total water for each grid, and their frequency in each bin was accumulated. We show the standard deviation and skewness for each bin of averaged mixing ratio of total water for the PDF analysis.

Figure 12 shows the standard deviation and skewness profiles of grid-averaged mixing ratio of total water in a GCM grid scale. The standard deviation and skewness are $1.2\,\mathrm{g\,kg^{-1}}$ and 0.2, respectively, between 5 and $15\,\mathrm{g\,kg^{-1}}$ of GCM-grid averaged total water. Although each frequency distribution is different, e.g., there are peaky, double peak, and broad shaped distributions, the PDF shape should be attributed to the Gaussian distribution, if we suppose the bulk PDF of total water. This results show that the Gaussian distribution should be applied to the PDF in the large-scale condensation process.

The standard deviation is small for small mixing ratio of total water less than $5\,\mathrm{g\,kg^{-1}}$. This should be attributed to the effect of the lower limit of mixing ratio. The skewness has large positive values in this case. For small mixing ratio of total water, temperature should be quite low. Thus, it should be considered that the PDF expands to large mixing ratio due to the existence of ice particles, which has a small fall velocity. On the other hand, the standard deviation is also small, and the skewness has small negative values for large mixing ratio of total water larger than $15\,\mathrm{g\,kg^{-1}}$. This should be attributed to the effect of the upper limit of relative humidity. In this case, condensates should be liquid (rain), and they are removed from the grid quickly because of its large falling velocity. As a result, the PDF reduces on the larger side of mixing ratio.

These features are not varied for latitude and layers (height). However, those over the ocean are different from those over land, and a profile of standard deviation in winter differs from those in other seasons. More analysis is required using cloud resolving models to understand the PDF well, and to improve the large-scale condensation processes in the GCM.

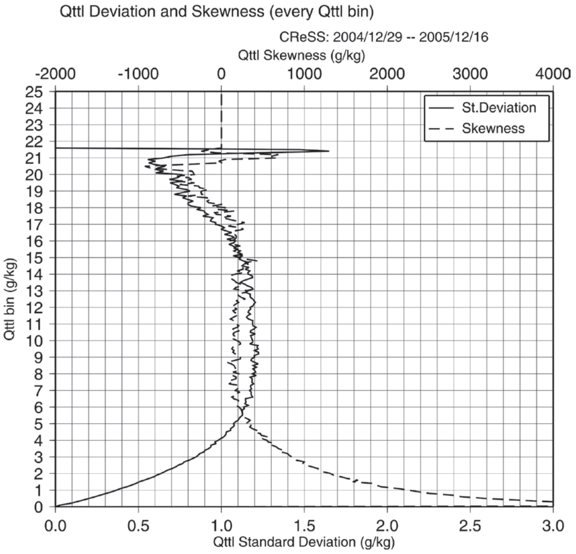

Fig. 12. Standard deviation (solid line) and skewness (broken line) profiles of mixing ratio of total water for the grid averaged one in a GCM grid scale. Skewness a thousandfold times is shown.

Characteristics of monsoon precipitation systems in and around Bangladesh during 2000–2005

We investigated the characteristics of precipitation systems for heavy rainfall in Bangladesh (88.05–92.74 deg.E, 20.67–26.63 deg.N), which is influenced by the Asian monsoon system. Precise understanding of the distribution and characteristics of precipitation systems is useful for disaster prevention and water management in an agriculture-dependent country like Bangladesh.

Six years of S-band weather radar data from 2000, obtained by the Bangladesh Meteorological Department, were used to reveal the characteristics of precipitation systems. Precipitation systems with a lifetime longer than three hours and a dimension larger than 100 km (long axis) were analyzed. We identified the shape, horizontal scale, propagation speed, and lifetime as the characteristics of precipitation systems. The precipitation systems were classified into Arc, Line, and Scattered types, according to their shape. The systems were divided according to the length of their long axis into small scale (SS, from 100 to 200 km), medium scale (MS, 200 to 300 km), and large scale (LS, larger than 300 km). Based on the propagation speed, the systems were divided into stationary (less than $2\,\mathrm{m\,s^{-1}}$), slow moving (2 to $7\,\mathrm{m\,s^{-1}}$), and fast moving (larger than $7\,\mathrm{m\,s^{-1}}$). The approximate lifetime of the systems was calculated from available scans.

The frequencies of the Arc-, Line-, and Scattered-type systems were determined to be 230 (29%), 117 (15%), and 442 (56%), respectively, from April to September during the analysis years. For the Arc-, Line-, and Scattered-type systems, the averaged horizontal scales were about 185, 184, and 268 km; propagation speeds were 11.0, 7.1, and $5.8\,\mathrm{m\,s^{-1}}$; and approximately lifetimes were 4.3, 4.0, and 4.8 h, respectively. The Scattered-type system dominated during the monsoon period (June, July, August, and September), while the Arc-type dominated in the pre-monsoon period (April and May). The Line-type system had an almost equal frequency of occurrence in both periods. Systems that developed in the monsoon period were long and stationary or slow moving, whereas systems in the pre-monsoon period were small and fast moving. Systems in the pre-monsoon period propagated southeastward, whereas those in the monsoon season propagated northwestward, northeastward, and southeastward (Fig. 13).

This analysis discloses that the population of precipitation systems is high in the southern, eastern, and northern part of Bangladesh (Fig. 14). Of the total of 442 Scattered-type systems, 244 covered a wide area, which was beyond radar range, and moved slowly. We called these systems the Scattered-type systems having wide areal coverage (SWAC). This analysis revealed that about 97% of the SWAC developed during the monsoon period and it made a huge contribution to monsoon rainfall in this region.

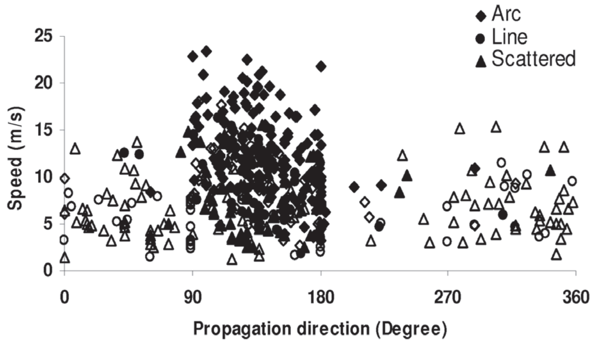

Fig. 13. Propagation speed and direction of different types of systems. The precipitation systems whose propagation speed was not observed and the SWAC are not shown. Solid and open symbols represent the systems that developed in the pre-monsoon and monsoon periods, respectively.

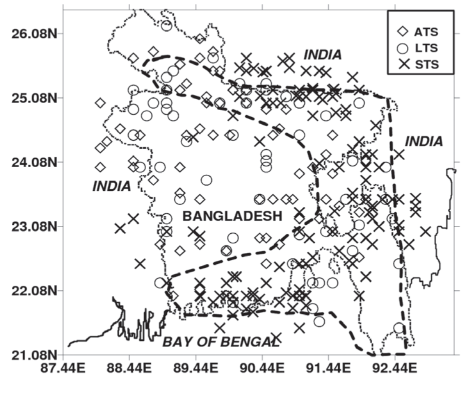

Fig. 14. Spatial distribution of different types of systems that developed in and around Bangladesh during the monsoon period. The dashed line represents the wet region presented by Islam and Uyeda (2007). The SWACs are not shown.

Laboratory for Climate System Study

Intraseasonal variability in diurnal rainfall over New Guinea and surrounding oceans during austral summer

High-resolution Tropical Rainfall Measuring Mission (TRMM) rainfall data for six wet seasons (December–March) were used to investigate the time and space structure of the diurnal cycle of rainfall over and around New Guinea (Fig. 1), a major island of the Maritime Continent. Here, our particular focus is on the modulation of the diurnal cycle associated with intraseasonal variability in the large-scale circulation pattern, with regimes associated with low-level easterlies or westerlies over the island.

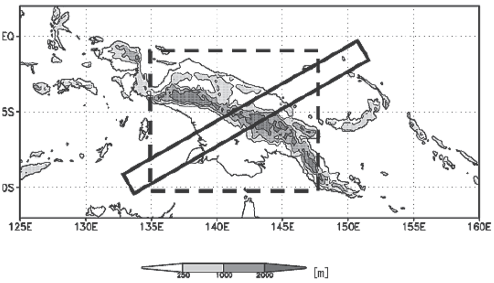

Fig. 1: Orography over New Guinea. The cross-island rectangle denotes the calculation domain for the time-distance cross diagrams in Fig. 3. The dashed rectangular box shows the area within which the time series of area-mean zonal wind were calculated to define the wind regime.

Figure 2 shows the composite mean rainfall distribution and 850-hPa wind for each regime over and around New Guinea. The detailed characteristics of the daily rainfall distribution and low-level wind pattern change greatly between the two regimes. In the easterly regime, the easterly from the Pacific changes to northwesterly across the equator northeast of the island. Wind is weak northeasterly over the island. Rainfall is concentrated over the south–southwestern side of the island, where low-level winds weaken and converge. Rainfall is not observed over the windward (northeastern) side of the island but it is localized over land areas in northern Australia. In contrast, during the westerly regime (Fig. 2b), strong northwesterlies prevail over the island. The distribution of rainfall is widespread, especially over the northeastern–eastern side of New Guinea, which extends eastward from the island to the equatorial southern Pacific under the low-level westerlies. Enhanced offshore rainfall is prominent off the northeast coast near New Britain Island (east of New Guinea). Significant rainfall can also be seen over the offshore area to the south of New Guinea, spreading from northern Australia in association with a cyclonic circulation.

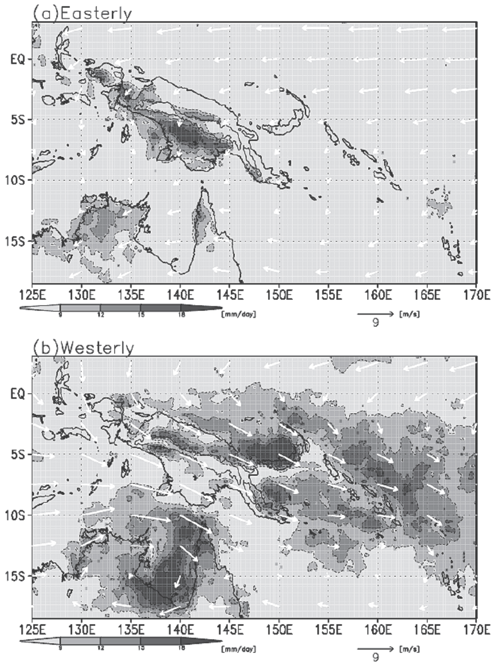

Fig. 2: Composite rainfall distribution and wind at 850 hPa for each wind regime (a: easterly; b: westerly). The orography is shown by the 1500-m contour.

Figure 3 shows a time–distance cross section for a domain perpendicular to the central mountain range of New Guinea (Fig. 1) to highlight the differences in diurnal rainfall under the different wind regimes. A striking feature of the diurnal variability in the regimes is that rainfall activity is propagated southwestward (northeastward) in the easterly (westerly) regime. Under both regimes, rainfall develops in the afternoon over the central mountain range and subsequently propagates to the northeast/southwest lowland areas with a phase speed of 2 to 3 $\mathrm{m\,s^{-1}}$. In the easterly regime, the rainfall spreads offshore during the morning but is localized near the coast and gradually dissipates. In the westerly regime, significant rainfall propagates in the offshore area northeast of the island. The rainfall propagates faster over water than over land, with an inferred phase speed of about 7 to 8 m s^{-1}. Offshore propagation continues until the following day and is linked to the afternoon peak in rainfall over the open Pacific. Moderate rainfall also occurs over the southwestern part of New Guinea during the westerly regime. Over southwestern New Guinea, rainfall propagation from the central mountain range weakens at night, but offshore rainfall then spreads from north of Australia to New Guinea.

The development and propagation of diurnal rainfall would occur as large-scale circulations interact with local circulations induced by orography. Further detailed investigation is warranted to reveal the processes that organize convection, including numerical simulations using high-resolution cloud-resolving models.

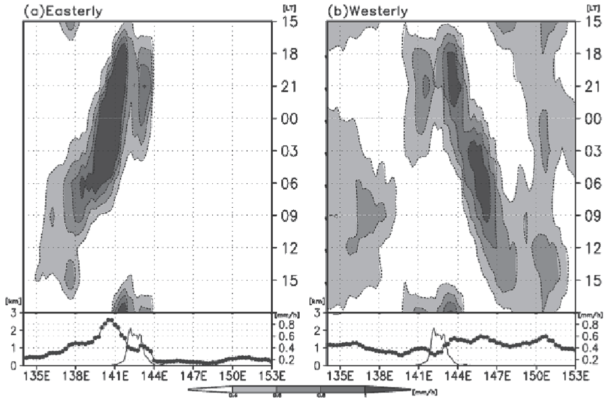

Fig. 3: Time distance cross sections of regime rainfall along the cross-island rectangle in Fig. 1 averaged in the domain perpendicular to the central mountain range (a: easterly; b: westerly). Land terrain (solid line) and daily accumulated rainfall (solid line with open circles) are described at the bottom of each diagram.

Interannual variability of atmospheric water balance over South Peninsular India and Sri Lanka during the northeast monsoon season

We have investigated the atmospheric water balance over South Peninsular India and Sri Lanka (PEN and SL) during the months October to December (OND) using computed moisture convergence (*C*) and residual evaporation (*E*) from NCEP/NCAR reanalysis data and GPCP precipitation data.

The monthly annual rainfall pattern has a double peak: the first in June and another in October. The second peak around October is the northeast monsoon rainfall (NEMR). The atmospheric water budget during the NEMR season over the domain (Fig. 4(b)) during the NEMR months (OND) is favored by higher evaporation throughout the season. Evaporation almost equals precipitation throughout the rainy season ($E \sim P$) (Fig. 4(b)). Most earlier studies have shown that the ocean acts as a source of moisture during the NEMR monsoon months for this domain. Here, we have found that the contribution to precipitation (*P*) during the OND months is also significant. The contribution of evaporation to mean seasonal precipitation is high over the PEN and SL region during the NEMR monsoon period and also for interannual variability, the correlation between *P* and *C* is 0.73 (exceeds 95% significant level) and the correlation between *P* and *E* is 0.84 (exceeds 95% significant level) (Fig. 4(c)); thus, the contribution of evap-

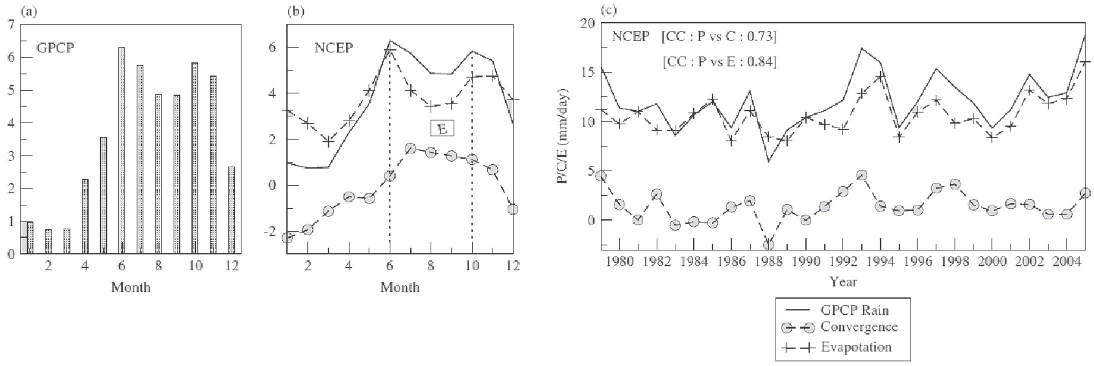

Fig. 4: Observed monthly mean annual cycle of *P*, *C*, and *E* over the selected domain for the period 1979–2005. (a) GPCP precipitation; (b) *P*, *C*, and *E* and (c) interannual variability (OND) of *P*, *C*, and *E* over the selected domain (values of correlation coefficients between *P* & *C* and *P* & *E* are shown in the graph).

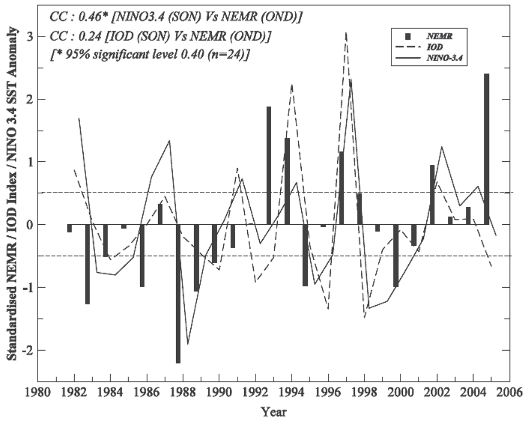

Fig. 5: Standardized anomalies of NEMR over the selected domain during OND. IOD indices during SON and NINO-3.4 SST anomalies during SON from 1982 to 2000. IOD: Difference in SST between western Indian Ocean (10S–10N, 55E–70E) and Southeast Indian Ocean (10S–0N, 90E–120E); NINO-3.4: 5S–5N, 190E–240E SST anomalies.

oration during the monsoon months to the year-to-year variability of precipitation has clearly been brought out through the atmospheric water budget, i.e. ($E > C$). The correlation between precipitation and residual evaporation at 0.84 suggests that the land surface hydrological process is also important to understand the P variability on interannual timescales over this region. During OND, strong land–atmospheric interactions co-exist over this region along with ocean–atmospheric interactions.

NEMR variability is influenced by various climate anomalies (e.g., El Nino/La Nina and Indian Ocean Dipole (IOD)). Figure 5 shows the times series of NEMR (filled bar) over the selected domain (PEN and SL) during OND, IOD index (dashed line) during September – November (SON), and NINO-3.4 sea surface temperature (SST) anomalies (solid line) during SON from 1982 to 2000. The correlation coefficient between NEMR and IOD is found to be less than the significance level (0.24), whereas the correlation coefficient between NEMR and NINO-3.4 anomalies is significant (0.46) at the 95% significance level. It has been noted that positive NEMR is associated with El Nino coupled with IOD, but negative NEMR is weakly associated only with La Nina over PEN and SL.

The regressed pattern of precipitation reveals a significant negative relationship with the Indo-China Peninsula precipitation during the NEMR monsoon (OND) season (Fig. 6(a)). A significant positive correlation (95% significance level) over the Nino-3.4 regions and over the Bay of Bengal near Myanmar coast and South China Sea, and a less-than-significant negative correlation over Southeast Indian Ocean over the coast of Sumatra are noted and no correlations are observed with IOD. Figure 6(c) shows that the convergence over IO is significantly associated with domain precipitation and the moisture flux vectors largely originate from the southeastern Indian Ocean region. Figure 6(d) shows that evaporation also plays an active role in modulating the interannual variability of NEMR precipitation over the PEN and SL domains.

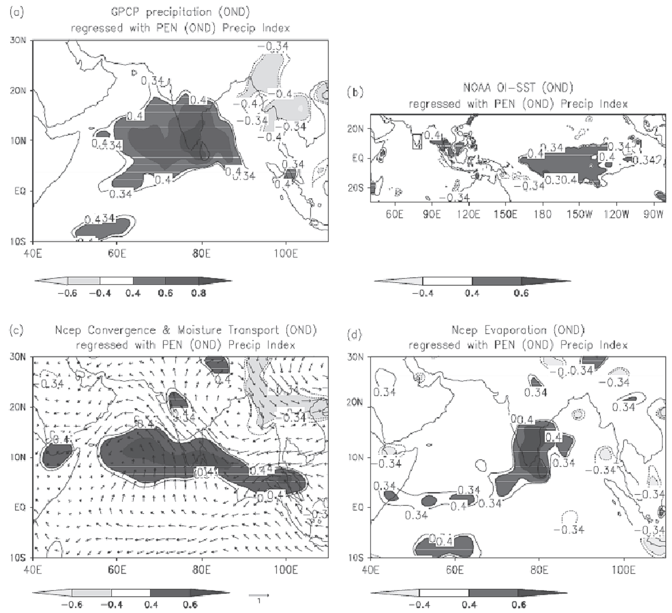

Fig. 6: Regression maps based on PEN and SL domain GPCP precipitation. Top panel: (a) GPCP precipitation, (b) OND SST (domain encompassing PEN and SL is shown by a box). Lower panel: (c) NCEP moisture convergence and moisture flux transport, (d) NCEP evaporation (95% significance levels are shaded and only the 90% level is contoured).

Dominant interannual and decadal variability of winter surface air temperature over Asia and the surrounding oceans

In recent decades, mid- and high-latitude regions of continental Asia in winters have shown the strongest global warming. In this study, we extract the dominant spatiotemporal pattern of surface air temperature (SAT) variabilities during winter in the high latitudes through the tropics over the whole of Asia and the surrounding oceans, and examine the associations of these patterns with some climate variables, using NCEP/NCAR reanalysis data. We employed air temperature at the 0.995 sigma level as SAT.

We applied principal component analysis to normalized monthly SATs. The first mode represents the Asian north–south dipole pattern with a node over the Tibetan Plateau (Fig. 7). This component has close relationships with the Arctic Oscillation, and cold-surge variability around Southeast Asia, showing decadal oscillation with signal changes in 1988 and 1997. The second mode is the Inner-Asian mode with a center to the north of the Tibetan Plateau (Fig. 8). This component connects to fluctuations of not only the western Siberian high but also the Icelandic low, which is associated with the pattern of the polar vortex over Eurasia. A recent warming trend and possible relationship with solar activity are also shown. The modes of Asian SAT variability associated with ENSO are extracted as the north-south dipole mode over the tropical western Pacific and Japan (the third mode) and Silk Road mode (the fourth mode). The two independent modes appear to be caused by different sea surface temperature (SST) anomalies over the Pacific and Indian Ocean and their associated atmospheric Rossby-wave responses. The linkage of tropical SST and atmospheric circulation over the western Pacific and the Indian Ocean could contribute to the maintenance of wave trains both north and south of the Tibetan Plateau in the third mode, whereas extremely large ENSO induce the atmospheric wave train, which propagates toward the Silk Road via Greenland in the fourth mode.

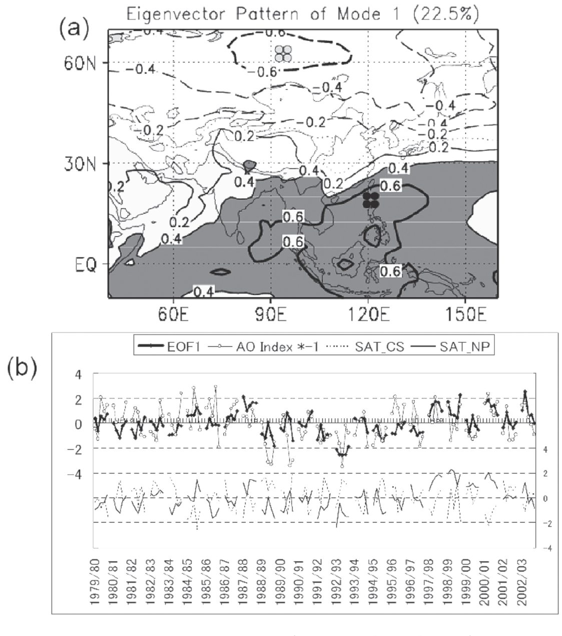

Fig. 7: First component of normalized surface temperature anomalies in winters from 1979/80 to 2002/03. (a) Eigenvector patterns. (b) Top: Time series of the score (thick line). The AO Index multiplied by –1 (thin line) is superimposed. Bottom: Time series of normalized SAT around the extreme value of the eigenvector. Solid (dashed) line is the average of four grids located in the positive (negative) area over Northern Philippines (Central Siberia), shown as closed (open) circles in (a).

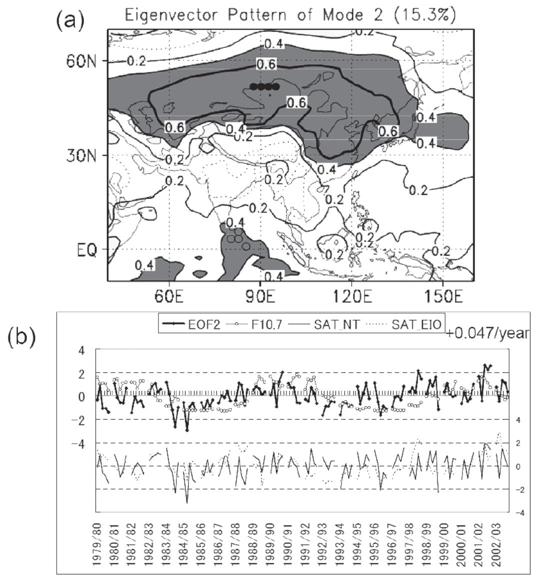

Fig. 8: Same as Fig. 7 but for the second component. Solar flux (F10.7: thin line) is superimposed in the top of (b). In the bottom of (b), the solid (dashed) line is the average of four grids located in the positive area over Northern Tibet (Equatorial Indian Ocean), shown as closed (open) circles in (a).

Laboratory for Cloud and Precipitation Climatology

An Observational Study of Tropical Convective Variability

A family of tropical clouds contains a rich variety of convective systems ranging over a broad spectrum from shallow cumulus to deep convection. Clouds are often observed in formation, or as how researchers prefer to say, “organized” in a system. A good example is a mesoscale convective system (MCS), in which deep convective cores are typically accompanied by shallow cumulus on the leading edge and trailing stratiform precipitation. A similar pattern of convective organization also appears in a synoptic-scale cloud system coupled with equatorial atmospheric waves, such as the Madden-Julian Oscillation (MJO). In this study, a 10-year record of global-scale observations is analyzed to explore the systematic variability in convection associated with individual modes of the equatorial waves. Tropical Rainfall Measuring Mission (TRMM) satellite data are used to separate shallow, cumulus congestus, deep stratiform, and deep convective systems. Changes in the dynamic and thermodynamic environments accompanying the convective variability are also investigated.

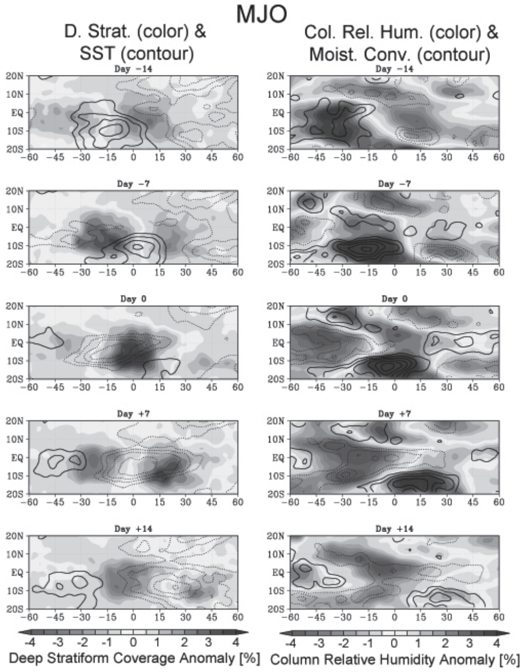

Fig. 1 Lagged composite analysis for the MJO, with days marked as –14 to +14 from top to bottom:
Left: Deep stratiform coverage (shaded) with SST (contour).
Right: Columnar relative humidity (shaded) with moisture convergence (contour).

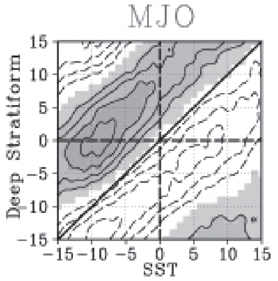

Fig. 2 Lagged correlation diagram comparing the deep stratiform coverage and SST. Shaded areas show positive correlations. Labeled numbers represent date.

The lagged composite diagram for the MJO (Figure 1) captures a preceding increase in sea surface temperature (SST) and the preconditioning of humid environment brought by moisture convergence. These are likely to give rise to the MJO convective peak. Such lagged correlations are more quantitatively assessed in Figure 2, where the highest correlation between SST and deep stratiform coverage appears 10 days before the MJO convective peak. In Figure 3, a similar correlation diagram is plotted for shallow and cumulus congestus clouds with respect to deep stratiform systems. Shallow and cumulus congestus systems develop a day or two earlier than the MJO convective peak. In contrast, non-precipitating high clouds are most extensive slightly after the convective peak (not shown). These results imply that convective systems associated with the MJO gradually develop in depth toward the convective peak, leaving behind cirrus clouds detrained from deep convective clouds. Figure 4 summarizes these findings.

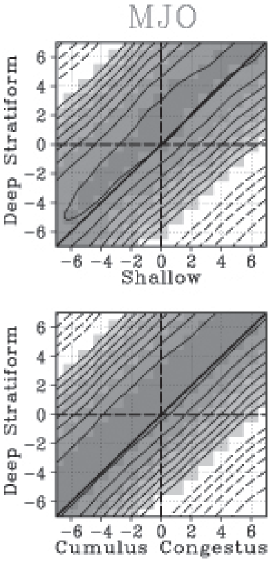

Fig. 3 Same as Fig. 2 except for shallow (top) and cumulus congestus (bottom) instead of SST.

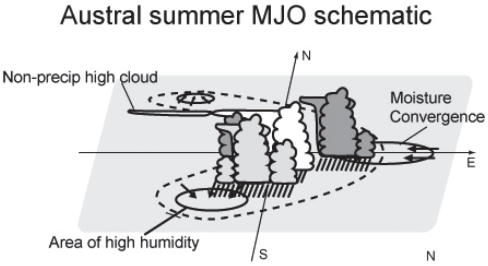

Fig. 4 Schematic diagram of the MJO as inferred from the present findings.

Evaluation of a global cloud-resolving model using satellite data

The Tropical Rainfall Measuring Mission (TRMM) Precipitation Radar (PR) and CloudSat Cloud Profiling Radar (CPR) provide unprecedented tools for detailed measurements of the structure of cloud and precipitation systems over the globe. Efforts are underway to develop next-generation global atmospheric models in which convective clouds are explicitly simulated in conjunction with general circulation. Progress in satellite remote sensing and model capability could bring breakthroughs in outstanding problems involving interactions between the cumulus convection and planetary-scale dynamics. One such challenge is the Madden-Julian Oscillation (MJO).

In this study, cloud and precipitation properties associated with the MJO are investigated for 32 days starting from December 15, 2006, based on a joint analysis of a global cloud-resolving model (GCRM) simulation and satellite measurements. The GCRM simulation used in this study is provided by the Nonhydrostatic ICosahedral Atmospheric Model (NICAM). Radiative transfer calculations were applied to the NICAM output to simulate 13.8- and 94-GHz radar reflectivities and 10.8μm brightness temperature. The synthesized “observations” make the NICAM outputs directly comparable with the TRMM and CloudSat measurements. The MJO was extracted by a time-longitude bandpass filter applied to TRMM observations. Composite analysis was then performed around the (spatially variable) base point defined at the ridge of the filtered MJO.

The composite diagram shows that the GCRM reproduces a slow, eastward propagation of convective areas very similar to the satellite measurements. Contoured frequency by altitude diagrams (CFADs) are constructed individually for wet and dry phases of the MJO, i.e., the portions where the filtered MJO is greater than 2σ or less than -2σ. The TRMM and CloudSat CFADs (Figures 5 and 6, respectively) both imply that deep convection prevails in the wet phase while shallow clouds are more dominant in the dry phase. The model-synthesized CFADs exhibit a qualitatively similar pattern, although the GCRM tends to overproduce deep convection, particularly in the MJO dry phase. The joint histogram of the cloud top and precipitation top confirms the excessive production of snow in deep convective clouds simulated by the GCRM. A sensitivity study suggests that a microphysical parameterization with less snow production, and perhaps with smaller particles for a given mixing ratio as well, would improve the model performance.

This study was conducted in collaboration with Prof. Masaki Satoh at the Center for Climate System Research, University of Tokyo, and Dr. Hiroaki Miura at the Frontier Research Center for Global Change, Japan Agency for Marine-Earth Science and Technology (JAMSTEC).

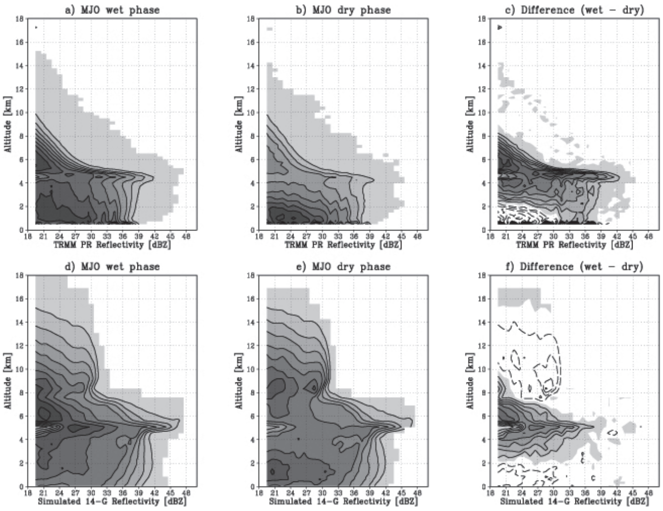

Fig. 5 TRMM PR CFAD for the MJO wet phase (left), dry phase (middle), and their difference (right). Dashed contour shows negative values.
Top: Observed; *Bottom*: Simulated.

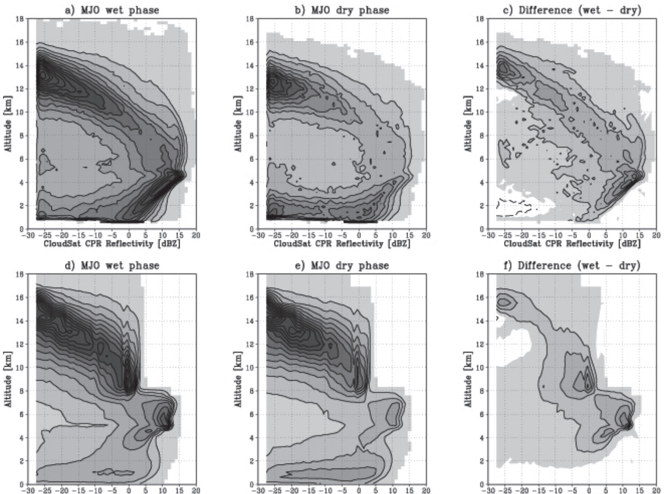

Fig. 6 Same as Fig. 1 except CloudSat CPR.

Laboratory of Satellite Meteorology

Study of algorithms for next-generation space-borne precipitation radar

The Global Precipitation Measurement (GPM) mission has been proposed as the successor to the Tropical Rainfall Measuring Mission (TRMM). The core GPM satellite will be equipped with a microwave radiometer (GMI) and a dual-wavelength radar (DPR). The combination of DPR and GMI data may improve retrieval of instantaneous precipitation rate. The main objective is to improve DPR precipitation retrieval using GMI data. The development of an algorithm for working with the data has begun. The dropsize distribution, which is important for rain retrieval using radar, is assumed to have two parameters. The formulation and coding of the algorithm are complete, and its convergence characteristics and stability are under investigation. Prototype test data have also been constructed using a polarimetric radar located in Okinawa Island. Using relationships between polarimetric signatures and the dropsize parameters obtained from ground-based disdrometer measurements, the polarimetric signatures were converted to drop-size parameters.

Study of precipitation system climatology over mountainous regions using TRMM data

Mountainous regions, such as the Himalayas and Andes, exhibit distinct precipitation characteristics, and diurnal variation is one of them. TRMM data covering more than nine years can be used to obtain not only fine-scale rain distribution but also diurnal signatures within the seasonal march. The extended time span covered by the data overcomes the poor sampling of the precipitation radar (PR) and enables us to obtain a detailed precipitation distribution.

The investigation results are twofold. The first involves precipitation system climatology over mountainous regions. This work fully utilized the long-term TRMM data. The second result involves the effect of topography, including that of lakes, on diurnal variation in precipitation.

Figure 1 shows the local time distribution of the maximum precipitation. Generally, the land receives afternoon/evening rain, and the ocean receives morning rain. There are excep-

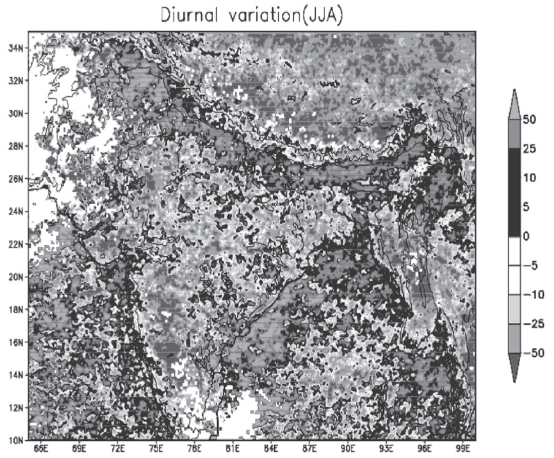

Fig. 1 Local time distribution of peak precipitation during June–August using TRMM eight-year precipitation radar data (1998–2006). Afternoon/evening rain is dominant over the Deccan Plateau and the Tibetan Plateau, while morning rain is evident in the southern foothills and the Bay of Bengal. The northern edge of the morning rain, near the Himalayas, shows clear topographic effects.

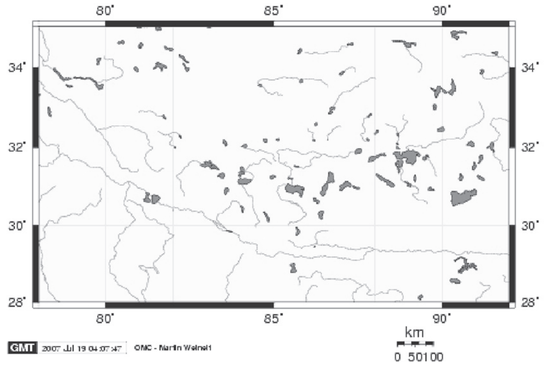

Fig. 2 Distribution of lakes in the Tibetan Plateau

tions such as the southern foothills of the Himalayas and the basin in Myanmar, which receive morning rain. The close-up images (Fig. 2) show many lakes distributed over the Tibetan Plateau, and the locations of the lakes coincide with areas where the differences between morning and afternoon rainfalls are large (Fig. 3).

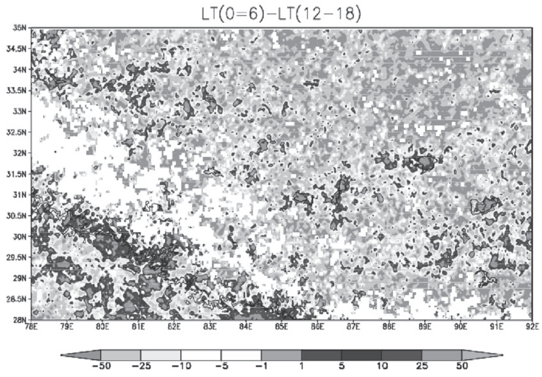

Fig. 3 Distribution of rain differences at 0–6 and 12–18 hours local time. Enhanced morning rain can be observed over the lake region.

Characteristics of low-level jets over Okinawa in the Baiu season using a 400-MHz wind profiler radar

Hourly observations from the 400-MHz wind profiler during the warm season for three years were used to develop climatology of the low-level jet (LLJ) over Okinawa, a Japanese subtropical island. Long-term wind observations with high temporal and vertical resolution allowed investigation of LLJ statistics. Characteristics of the LLJ are examined in two subperiods: during the Baiu season over Okinawa Island and in the post-Baiu season when the Baiu front has moved north of the site. The results show that the stronger LLJs occur more frequently during the Baiu sub-period, when heavier precipitation is observed mostly, compared with the post-Baiu sub-period. The distribution of the jet height and the mean wind structure are constructed and compared for the rainy and rain-free cases to clarify the features of the LLJs in association with the precipitation. Statistically, the frequency of LLJ occurrences exhibits a diurnal cycle, with most of them occurring in nighttime and early morning hours (Fig. 4). Interaction between the LLJ and the diurnal variations in the precipitation band was also suggested.

This observation was conducted as part of collaborative activity between HyARC and the National Institute of Information and Communications Technology (NICT).

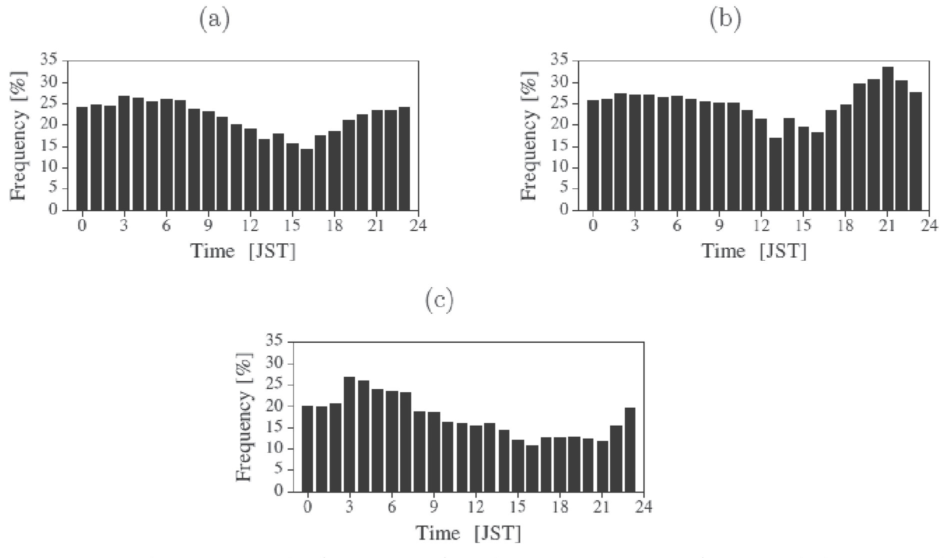

Fig. 4 Diurnal variation in the frequency of weaker LLJ occurrences for (a) total, (b) Baiu, and (c) post-Baiu seasons from three months of the three-year record (2004–2006).

Laboratory of Eco-Hydrometeorology

Characteristics of atmospheric turbulence observed in the surface and mixed layers over the Huaihe River basin in China

To elucidate the characteristics of atmospheric turbulence within the surface layer (SL) and the mixed layer (ML), dominant eddy scales were examined using the turbulent variables of three components (longitudinal velocity, lateral velocity, and vertical velocity) observed in both the layers (Figure 1). The study was conducted at Shouxian, China, over a flat terrain in the middle reaches of the Huaihe River basin (32°37'N, 116°48'E).

In the near-neutral SL, horizontal wind velocity spectra showed two peaks: the SL turbulent eddy scale and the larger eddy scale. The results of the turbulent statistical analyses revealed that the larger eddy scale in the SL turbulence was height dependent. This suggested that the smaller eddies in the SL were associated with each other and then scaled up to larger eddies, equivalent to the ML turbulent eddy scale.

From the results of spectral analyses of horizontal wind velocity, the longitudinal eddy scale was determined to be around 1.5 times the atmospheric boundary layer (ABL) height, which corresponds to previous studies (Kaimal *et al.*, 1976). On the other hand, the lateral eddy scale was much larger than the longitudinal (Figure 2). The reason for this could be that the lateral wind velocity spectra could not represent the scale of roll convection, because the fluctuation of the lateral wind velocity was much smaller when the roll convection flowed longitudinally.

In ML, the vertical wind velocity spectra showed a larger eddy scale than those reported in previous studies (Caughey and Palmer, 1979). Larger-scale eddies often appeared when stability in the SL was near neutral and the horizontal wind in the ML was relatively strong. Peak frequency of the vertical spectrum was sometimes consistent with oscillation in the free atmosphere.

The ratio of wavelengths for the horizontal spectral peak in the SL and ML was calculated. The ratio gradually increased to around 0.6, in accordance with atmospheric instability within the SL. The eddy scale in the middle of ML was about 4 times the ABL height, while the eddy scale in the SL increased gradually from 1.0 to 2.5 times the ABL height when SL became unstable. This suggests that the coupling of dominant eddies between the ML and the SL was influenced by the SL's stability.

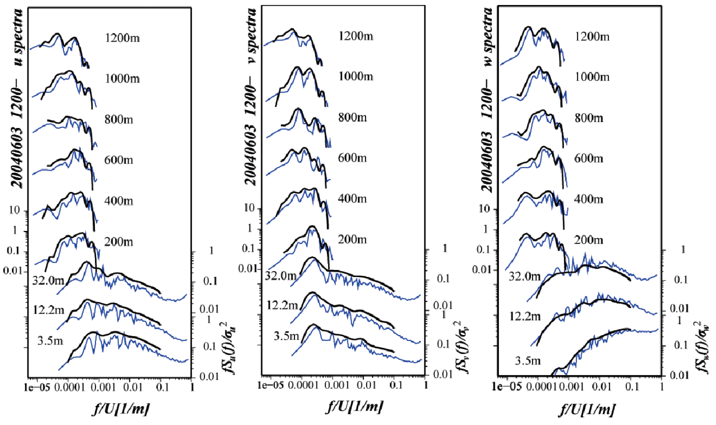

Fig. 1 Power spectra of three wind velocity components in the SL and the ML observed on 3 June 2004.
(*Left*: longitudinal velocity component; *Center*: lateral velocity component; *Right*: vertical velocity component).

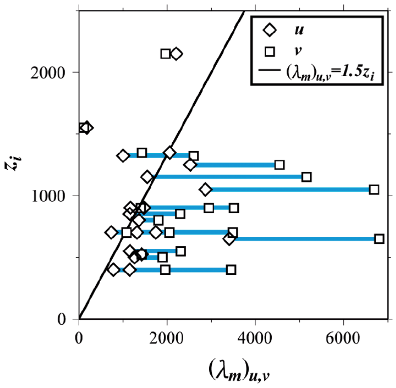

Fig. 2 Relationship between the ABL height (z_i) and the wavelength of the dominant eddy for horizontal wind velocities (longitudinal velocity components ◇, lateral velocity components □) in the SL.

Characteristics of atmospheric turbulence within the surface layer over the Loess Plateau in China

We present the power spectra of wind velocity and the cospectra of momentum and heat fluxes observed for different wind directions over flat terrain and a large valley on the Loess Plateau (Figure 3). The power spectrum of vertical (w) wind speed satisfies the –5/3 power law in the inertial subrange (Figure 4), but that of longitudinal (u) and lateral (v) wind do not vary as observed in previous studies conducted within low frequency ranges.

The u spectrum measured at a 32-m height for flow from the valley shows a power deficit at intermediate frequencies (Figure 5), while the v spectrum at 32 m downwind of the valley at 32 m reaches another peak in the low frequency range (Figure 6) at the same frequency as the u spectrum. The corresponding peak wavelength is consistent with the observed length scale of the convective outer layer at the site. The v spectrum for flat terrain shows a spectral gap at mid-frequencies while obeying inner layer scaling in its inertial subrange, suggesting two sources of turbulence in the surface layer. All the spectra and cospectra from the direction of the valley show a height dependency over the three levels.

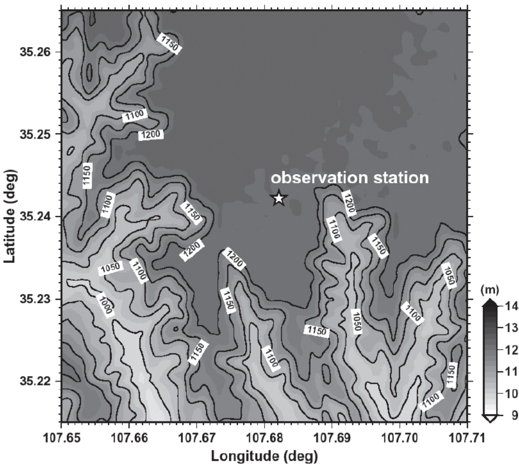

Fig. 3 The target area of the surface layer turbulence over the Loess Plateau in China.

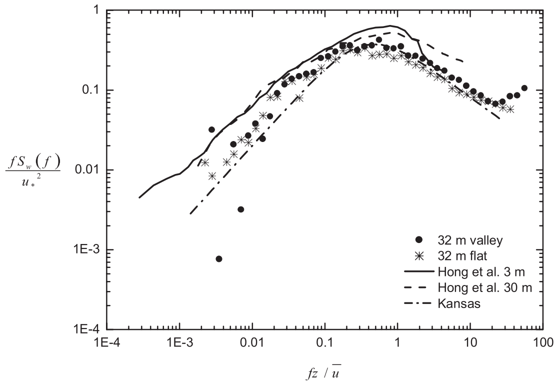

Fig. 4 Normalized power spectra of the vertical (w) wind component under near-neutral conditions using data from a 32-m height. The spectrum from the valley direction (●) is compared with that from flat terrain (✳).

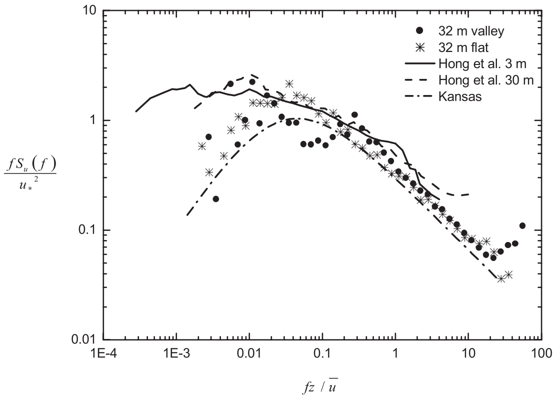

Fig. 5 Normalized power spectra of the longitudinal (u) wind component under near-neutral conditions using data from a 32-m height. The spectrum from the valley direction (●) is compared with that from flat terrain (✳).

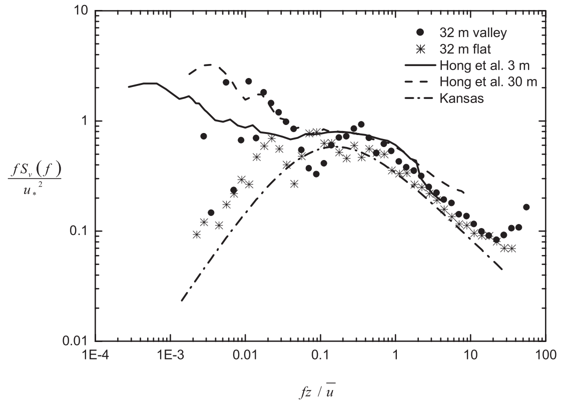

Fig. 6 Normalized power spectra of the lateral (v) wind component under near-neutral conditions using data from a 32-m height. The spectrum from the valley direction (●) is compared with that from flat terrain (✳).

Laboratory of Ocean Climate Biolgoy

The climate system surrounding us is governed by water and materials cycles in the hydrosphere and atmosphere on the Earth. In this laboratory, we aim to study the inter-relationship between climate change and ocean biogeochemistry on time scales ranging from a decade to century. Brief description of our laboratory activities follows.

● Ocean Primary Productivity Monitoring by Satellites

Primary productivity is one of the key processes in understanding the relationship between climate change and ocean biogeochemistry. A global view of the primary productivity can be attained by satellite remote sensing, however, its quantitative estimation is still hindered by lack of ground truth data on spatial and temporal scales. To fill this gap we developed, as a part of the Core Research for Evolutional Science and Technology (CREST) program 1999-2004, an ocean productivity profiling system using an underwater profiling buoy system and a custom made fast repetition rate fluorometer (FRRF). We are now developing a practical monitoring system of ocean primary productivity by operating the productivity profiling system in combination with supporting data handling systems to merge satellite and *in situ* data. This is under a new 5-year continuation project as a part of Solution Oriented Research for Science and Technology (SORST), started in 2004. The goal of the project is to design a system for monitoring global ocean primary productivity. The immediate task is to utilize satellite primary productivity data validated by the profiling buoy system for process studies on ocean biogeochemistry in response to physical forcing in order to demonstrate the usefulness of the validated satellite data.

Long-term operation of ocean productivity profiling system in central Sagami Bay

The underwater profiling buoy system is composed of an Underwater Winch System and a Profiling Buoy System. The Profiling Buoy is equipped with sensors and normally stays below the euphotic zone. It pops up to the surface on a pre-set schedule and measures the vertical profile from the winch depth to the surface then returns to the winch to await the next schedule. A custom made FRRF has been installed as the main sensor, in which data processing is conducted in real time during the profiling measurements. All measured data are stored with a part of the processed data being transmitted to the laboratory via cellular phone when the buoy pops up to the surface.

This instrument was operated three-times at the observation station S3 (St. S3) in central Sagami Bay in the fiscal year 2007. Here results from the long-term mooring from mid November 2007 to mid February 2008 are reported. The buoy operated as planned during this period despite the rough oceanic conditions that prevail in winter. Data collected from the system are shown in Fig. 1. During the entire period of observation, Chl a-specific gross productivity (Pbc) exhibited a subsurface maximum at a depth of around 300 μE m^{-2} s^{-1} of PAR while the subsurface Chl *a* maximum was located at a deeper layer (Fig. 1c, d). This implied that the photosynthetically produced particles (phytoplankton) are immediately removed from the upper layer by grazing and/or self-sinking, whereas they are efficiently accumulated below the productive layer. Time-series comparisons revealed that before Julian day 380 (day of year) peaks of Pbc were found a few days prior to Chl *a* peaks, whereas no such lag was observed when water mass properties changed after Julian day 380. Quantum yield of photochemistry (F_v/F_m D) was reduced accompanied with the increase in the mixed layer depth due to surface cooling, which may be attributed to the decrease in mean irradiance. This is the first-ever long-term (ca 100 days), continuous *in situ* measurement of ocean productivity, demonstrating the utility of our monitoring system for further understanding the natural variability of oceanic productivity.

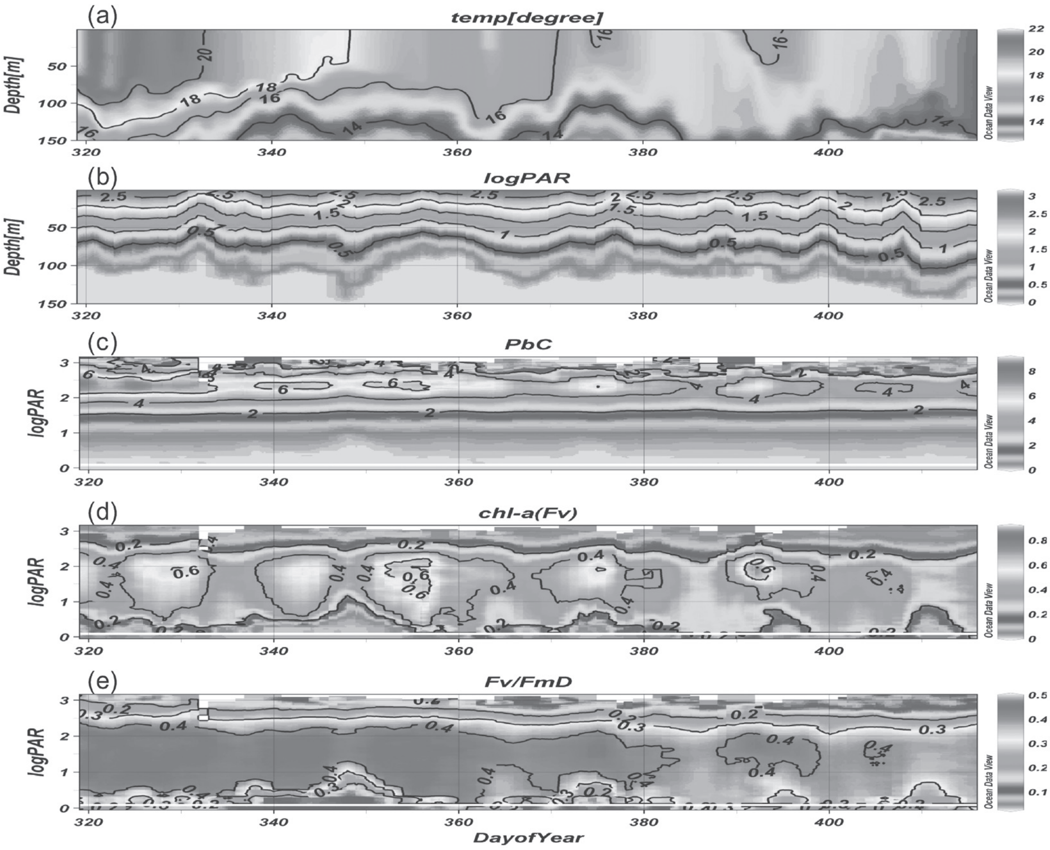

Fig. 1. Time-series data transmitted from the monitoring system in central Sagami Bay during Nov. in 2007 to Feb. in 2008. Measurements were conducted at noon. (a) Temperature, (b) Photosynthetically available radiation at noon (PAR; μE m^{-2} s^{-1}), (c) Chl a-specific gross productivity (Pbc; mgC $mgChl^{-1}$ h^{-1}), (d) Variable fluorescence (F_VD) corresponding to Chl a concentration, and (d) Quantum yield of photochemistry (F_V/F_mD).

Estimation of oceanic daily depth-integrated primary production from FRR fluorometry

In the operation phase, the ocean productivity profiling system conducts a few FRRF measurements per day, which provides depth-profile data of instantaneous Chl a-specific primary productivity (P^B_{O2}). In order to validate the satellite-derived productivity, it is essential to estimate the daily depth-integrated productivity. We have developed an algorithm to estimate the daily depth-integrated productivity from a single FRRF observation using the database obtained from the intensive time-series FRRF measurements in Sagami Bay (St. S3) during 2003-2006. Our algorithm, based on the day-to-day relationship between underwater PAR and P^B_{O2}, provides accurate estimates of daily depth-integrated productivity at St. S3. Moreover, the same algorithm was used to estimate the daily depth-integrated productivity at St. K2 (47°50'N, 160°00'E) in the western subarctic Pacific. There was good agreement between measured and estimated values at St. K2 (Fig. 2). This indicates that, by using the day-to-day PAR and P^B_{O2} relationship, our algorithm is effective for estimating daily pro-

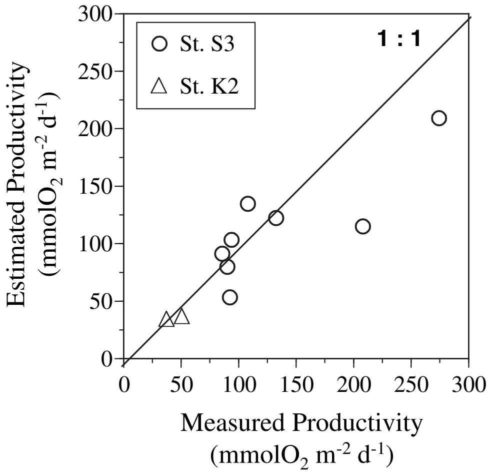

Fig. 2 Comparisons of daily depth-integrated productivity between intensive FRRF measurements and the algorithm-derived estimates.

ductivity and thus describing the varying physiological status of phytoplankton, which responds to small changes in oceanic conditions. This algorithm together with a single FRRF profile obtained from an ocean productivity profiling buoy system could assist in the monitoring of long-term daily depth-integrated productivity, which is of immediate need for the validation of satellite primary production models.

Physiological responses and productivity of marine phytoplankton assemblages determined from variable fluorescence quantum yields

Biological processes of phytoplankton in the ocean play a dominant role in controlling the global carbon cycle. Understanding the variability of phytoplankton physiological characteristics could enhance the ability to predict productivity, and thus lead to a better understanding of the role phytoplankton plays in global biogeochemical cycling. The present study examined the variabilities in physiology and productivity of natural phytoplankton assemblages in Sagami Bay from 2006 to 2007 using FRRF, and investigated the possible causes of the variations in physiological parameters in photosynthesis. Vertical profiles of photosynthetic parameters such as the functional absorption cross-section (σ_{PSII}) and photochemical quantum efficiency (F_v/F_m) showed distinct near-surface depressions. They could reflect the differences in the nutrient state of cells, as well as the light–dependent changes in their photosynthetic efficiency. Higher F_v/F_m observed in spring relative to that in fall suggested that cells of spring-dominant phytoplankton were in a better physiological state. Over shorter time scales, σ_{PSII} and F_v/F_m exhibited distinct diurnal cycles. Diurnal variation in σ_{PSII} could be a consequence of the adjustment of the absorption capability of cells – which is a photo-acclimation strategy. Decreases in the F_v/F_m were ascribed to the photoinhibitory process (photo-damage to PSII reaction center). This photoinhibitory process could be shown by F_v'/F_0'–, an indicative index for photo-damage, which markedly decreased around noon in both spring and fall populations of assemblages. The mid-day decrease was as high as 80% in spring compared to around 40% in fall. This implied that the photo-acclimation process and the degree of photo-damage differ among phytoplankton cells. For instance, the autumn phytoplankton assemblages with more effective acclimation capability sustained less damage under photo-inhibiting light intensities. The present study indicated that the FRRF-derived photosynthetic parameters of natural phytoplankton assemblages in Sagami Bay exhibited dynamic changes on scales ranging from diurnal to seasonal. These changes were closely associated with the photo-acclimation strategies of the dominant phytoplankton under variable light and nutrient availabilities. The varying productivity observed could be a result of the observed gradients in F_v/F_m and σ_{PSII}. The effect of environmental conditions on phytoplankton physiology observed using the FRRF technique could narrow the gap in our ability to estimate and predict primary productivity and thus provide significant insight into ocean biogeochemistry.

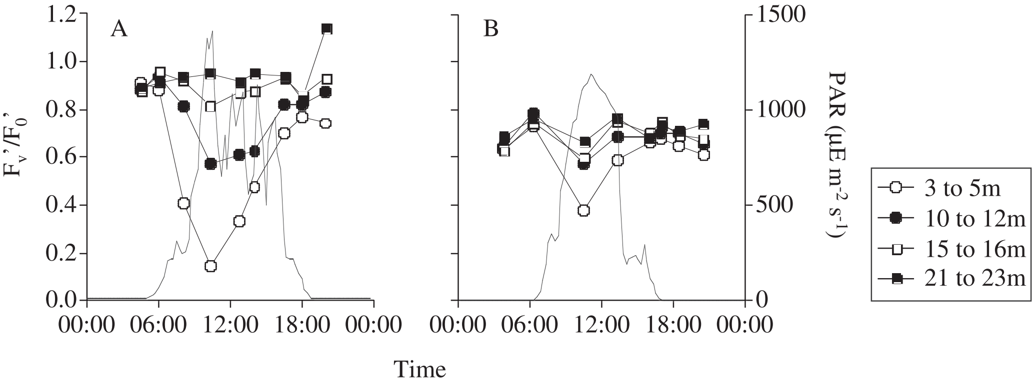

Fig. 3. Diel variation in F_v'/F_0' measured in natural phytoplankton assemblages in the Sagami Bay during May 2006 (A) and Nov. 2007 (B). Solid line indicates solar insolation.

Diel variations in the photo-physiological state of phytoplankton assemblages in the upper Gulf of Thailand

In coastal seas relatively high primary production occurs due to the supply of land-driven nutrients. The coastal primary productivity has large variability both in time and space in response to changes in environmental conditions caused by tidal movements, river inflow and human activities. In this study, intensive FRRF observations were conducted (2 hrs interval from 06/08:00 to 18:00) in the upper Gulf of Thailand (UGOT) in July 2006, to evaluate diel changes in the photo-physiological state of natural phytoplankton assemblages. Here we report the measurements of the functional absorption cross-section of PSII (σ_{PSII}), obtained from the eastern and western sites of the UGOT (St. 1 and 5, respectively). In the stratified upper column of St. 1 σ_{PSII} ranged from 340 to 820 Å^2 photon^{-1}, and from 480 to 900 Å^2 photon^{-1} in the well-mixed waters of St. 5. The relatively low σ_{PSII} at St. 1 implied that high light-adapted taxa with a high amount of non-photosynthetic pigments dominated, since they could be sustained under high light levels due to the strong halocline developed below. In both regions σ_{PSII} showed distinct diurnal variations, that is, midday decreases and evening recoveries. These variations were strongly correlated with variations in underwater PAR, which is attributable to the reversible, energy-dependent cycling of xanthophylls pigments in the PSII antenna. This process acts to dissipate excitation energy and hence protect RCII from photo-damage. The midday decreases in σ_{PSII} corresponded to ca 40% and 30% of potential values at St. 1 and 5, respectively. This indicated that cells at St. 1 had a more effective strategy for acclimation to a high light environment. On the other hand, it was also found that, even when the irradiance was the same, σ_{PSII} in the early morning and evening (06-08:00, 16-18:00) were higher than daytime values (10-14:00) (Fig. 4). This was clearly illustrated by the positive σ_{PSII} residuals from the site-specific regression curve with PAR in the morning and evening (Fig. 5a). These positive residuals appeared to be timed to relatively strong tidal mixing (Fig. 5b) that could bring deeper phytoplankton into the upper layer. Therefore, the observed higher σ_{PSII} in the morning and evening might result from inputs of cells acclimated to relatively low light with higher σ_{PSII} into the upper phytoplankton assemblages due to the periodically enhanced mixing. This result revealed the significance of changes related to tidal mixing in the photo-physiological status of phytoplankton assemblages and that it is one of the factors controlling diel variations in productivity in shallow coastal regions.

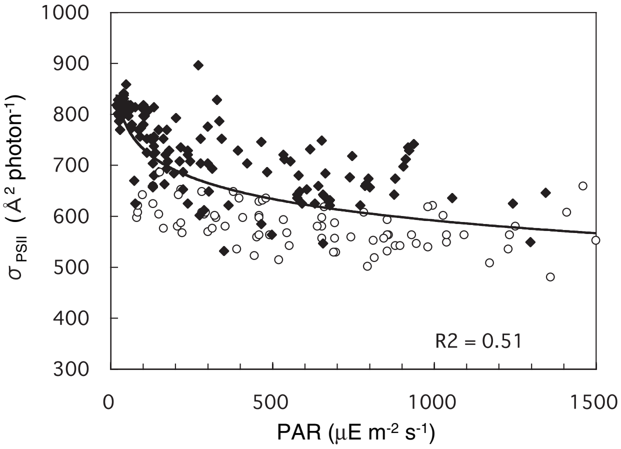

Fig. 4 Relationship between underwater PAR and the functional absorption cross-section of PSII (σ_{PSII}) of phytoplankton assemblages at the western site (St. 5) of the upper Gulf of Thailand. Symbols ◆ and ○ indicate the measurements in the early morning/evening (08:00, 16-18:00) and daytime (10-14:00), respectively.

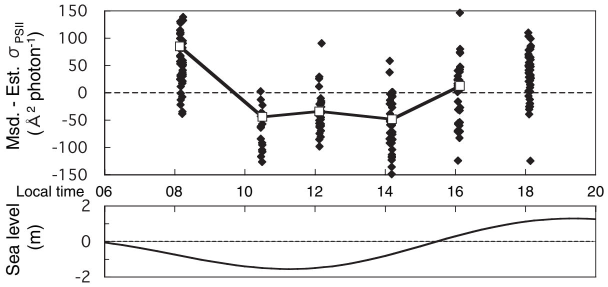

Fig. 5 (a) Diel variations in σ_{PSII} residuals from site-specific regressions with PAR (measured minus estimated σ_{PSII}). Symbol □ indicates the mean residual at each time.

(b) Diel variations in sea levels (m) on the observation day, calculated using local tidal harmonic constants. Tidal current and tidal mixing are enhanced at the time the sea levels of 0 m.

● Studies on changes in biogeochemical cycling in the ocean with reference to climate change.

Estimation of surface water pCO_2 in the East China Sea

In recent years much attention has been paid to the efficiency of CO_2 absorption on the continental shelf. But observation of the surface seawater partial pressure of CO_2 (pCO_2) has been limited by coarse spatial and temporal scales; therefore, seasonal variations of CO_2 absorption have not been well understood. This study aims to reveal pCO_2 distribution in the East China Sea (ECS) on a monthly time resolution. For this purpose, year-round observations of oceanic carbonate parameters (pCO_2, total alkalinity (TA), and dissolved inorganic carbon (DIC)) were conducted around the Tsushima Straits located at the north-eastern edge of the ECS continental shelf. From these datasets, empirical relationships between carbonate parameters and physical and biological parameters (SST, salinity, and Chl a) were successfully obtained. By applying these relationships to satellite SST, Chl a, and climatological salinity, monthly pCO_2 distributions in the ECS were estimated. The estimated pCO_2 distributions showed clear seasonal variation (Fig. 6). During winter, pCO_2 remained low due to low SST, and while it increased toward summer along with rising SST. Meanwhile from June to September, increased freshwater input from the Changjiang River reduced salinity in the ECS, leading to locally lowered pCO_2. The estimated pCO_2 agreed well with previous observations in winter and summer, within an error of 4%, enabling rough estimation of seasonal air-sea exchange of CO_2 in the ECS. The ECS acts as a sink for atmospheric CO_2 throughout the year with higher absorption in winter (0.01-0.02 PgC/Jan.-Mar.) and lower in summer (0.003-0.005 PgC/Jul.-Sep). Yearly-averaged gas exchange is 0.02-0.04 PgC yr^{-1}, which amounts to 1/100-1/50 of the open ocean uptake though the areal coverage of the ECS is only 1/500 of the world ocean, indicating 5-10 times higher efficiency than the open ocean CO_2 sequestration.

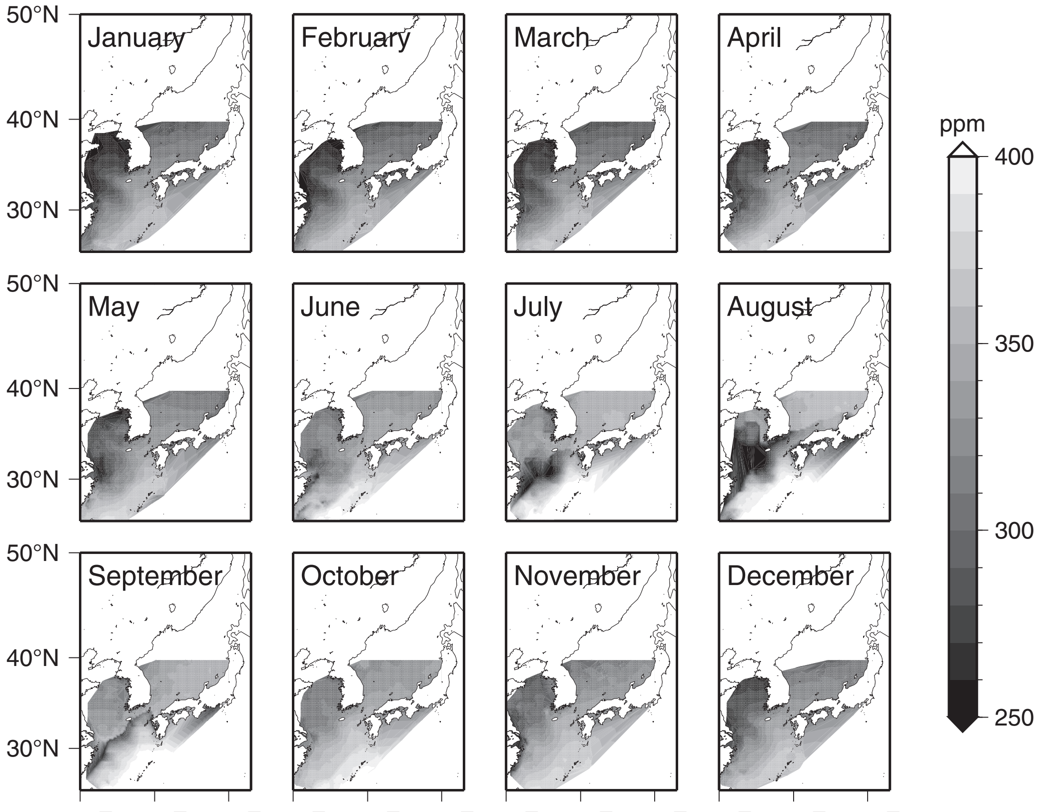

Fig. 6. Monthly surface pCO_2 distribution in the East China Sea. The reference year (i.e. atmospheric CO_2 level) is set as year 2005.

Enhancements of chlorophyll a concentrations and primary productivity in the upwelling region northeast of Taiwan following the passage of episodic typhoons

It has been reported that the passage of a typhoon in the vicinity of Taiwan is able to displace the Kuroshio Current toward the shelf (<200 m depth). Such a landward movement of the Kuroshio Current can induce local upwelling of the Kuroshio subsurface water (usually located at depths from 50m to 400 m), which alters physical and chemical properties and thereby biological activities in the shelf waters. With the use of multiplatform satellite data and primary productivity (PP) model, this study aims to assess the variations in phytoplankton chlorophyll a concentrations (Chl-a) and PP in the region northeast of Taiwan (bordered by the dashed circle in Fig. 8c) in response to the passage of typhoons. In most cases of typhoon passage during 2002-2007, both Chl-a and PP increased, accompanied with a decrease in SST. The mean enhancements of Chl-a and PP over the study region inversely correlated with the post- and pre-typhoon sea surface temperature (SST) differences (Fig. 7). This indicates that typhoon-related upwelling of cold Kuroshio subsurface waters enhanced local productivity. Among the observed 12 typhoons, the highest Chl-a and PP enhancements were found after the passage of Typhoon Haitang (July 2005) with magnitudes of 1.06 mg m^{-3} and 1229 mgC m^{-2} d^{-1}, respectively (Fig. 1a, b). After Haitang, MODIS SST composite image (22–24 July) exhibited an obvious notable surface cooling in the region northeast of Taiwan with SST <24.0 °C (Fig. 2a), whereas before Haitang (12–16 July) the temperature ranged from 27.0 to 28.0 °C (Fig. 2d). Post-Haitang satellite Chl-a showed phytoplankton blooms with ranges of 2.0-4.5 mgChl m^{-3} (Fig. 2b), whereas only around 0.25 mgChl m^{-3} before Haitang (Fig. 2e). Remarkable PP enhancement (from 750-1500 to 1500-4500 mgC m^{-2} d^{-1}) was also observed as shown in Fig. 2c and 2f. From high frequency radar data, it was clear that, following passage of Haitang, the main axis of Kuroshio Current (gray vectors in Fig. 2g, h) was shifted toward the shallow shelf area, which induced an upwelling of cold, nutrient-rich waters which resulted in the consequent local phytoplankton blooms. The Kuroshio upwelling around northeast of Taiwan is generally accepted as one of the most important processes for nutrient supply into the East China Sea (ECS). The scale and/or frequency of the typhoon-driven upwelling such as observed could affect overall productivity in the ECS.

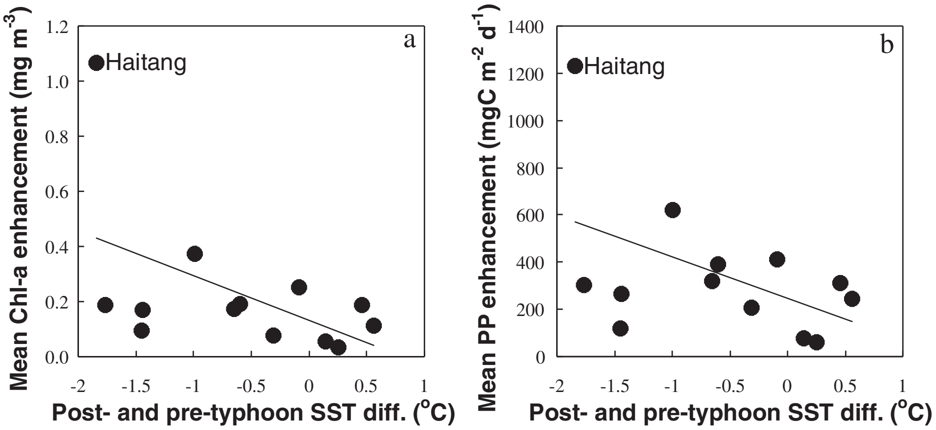

Fig. 7 Scatter plots of (a) mean Chl-a ($r = 0.51$, $p > 0.05$) and (b) PP ($r = 0.49$, $p > 0.05$) enhancements against post- and pre-typhoon SST differences. Solid line indicates linear least squares fit to the data.

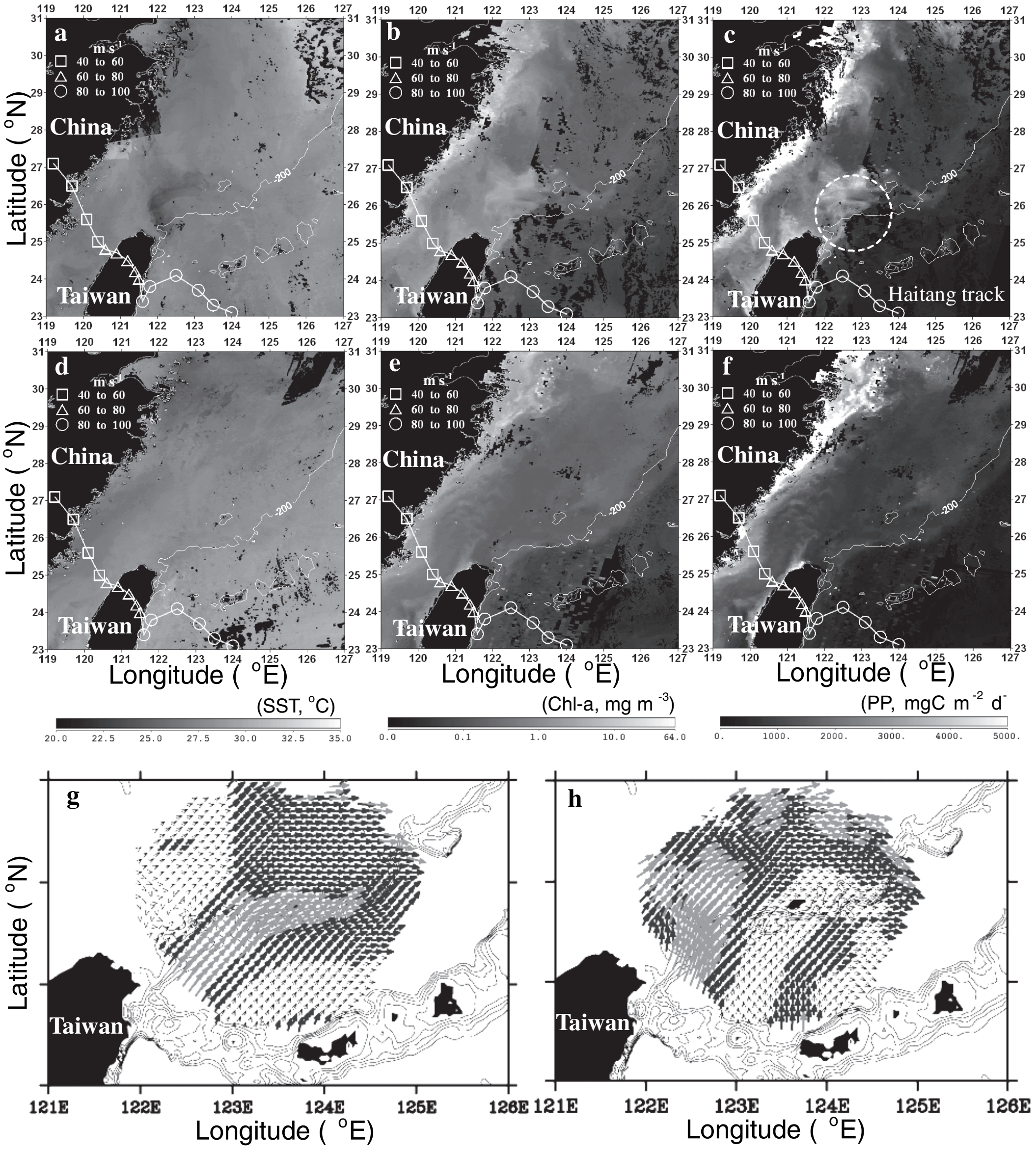

Fig. 8 Composite images of SST (MODIS), Chl-a (merged SeaWiFS and MODIS), estimated-PP and high frequency radar data showing Kuroshio main axis for before and after the passage of Typhoon Haitang. (a), (b), and (c) are for post-typhoon (22-24 July 2005) SST, Chl-a and estimated PP, respectively. The white curve indicates Typhoon Haitang trajectory with the track symbols of open square, triangle, and circle indicating the magnitude of maximum sustained wind (m s^{-1}). (d), (e), and (f) are the same as (a), (b), and (c) except that they are for pre-typhoon (12-16 July 2005). (g) and (h) show the Kuroshio Current speed derived from high frequency (HF) radar data for before (8-17 July 2005) and after Haitang (22 July 2005), respectively. Gray arrows indicate current speed >1 m s^{-1}.

Laboratory of Bio-Physical Oceanography

Evaluation of tidal error in altimetry data in the Asian marginal seas

Satellite altimeters have been measuring sea surface height since 1992, and the data have been used to study various oceanic phenomena such as eddy activity and temporal and spatial variations of sea surface currents. Since AVISO has been distributing corrected sea surface dynamic height anomaly data and its gird data, the satellite altimetry data is available. Although AVISO altimetry data include the data for the marginal seas, usage of these data is not recommended, primarily because of the large tidal error. However, AVISO altimetry data in the marginal seas have been used before confirming the tidal error. In the present study, we examine the accuracy of the AVISO altimetry data in terms of tidal correction in the Asian marginal seas, and then make a more accurate altimetry data set for those seas.

We used AVISO altimetry data from Topex/Poseidon, Jason-1, ERS-2 and Envisat, called CorSSH (Corrected Sea Surface Heights). The duration of the data was from December 1992 to February 2007. From these data, we constructed two data sets; in one, tidal signals were removed by a global tidal model (tidal signals corrected data) and in the other, tidal correction was not applied. The tidal correction was validated by spectral and harmonic analysis of the tidal signals corrected data set.

Spectral peaks corresponding to the tidal periods appeared in shallow water regions such as the Yellow and Okhotsk seas. This result indicates that the AVISO altimetry data in the shallow water regions involve a large tidal error. In order to see the spatial distribution of tidal error in the altimetry data, the amplitudes of four principal tides were calculated from the tidal corrected data set by harmonic analysis (Fig. 1). Since the data set already had the tidal signals removed, the calculated amplitude would be almost zero if the data did not contain the tidal error. The tidal amplitudes in the northern part of the Okhotsk Sea, the entrance to the Japan Sea, Yellow Sea, Luzon and Taiwan Straits, and around Kuroshio Extension were large. In the Kuroshio Extension, the tidal signals might be small because the water in the area is quite deep. Therefore, large tidal amplitudes in this area were not due to the tidal error. It is suggested that a large tidal error is involved in the AVISO altimetry data in the above areas except in the Kuroshio Extension.

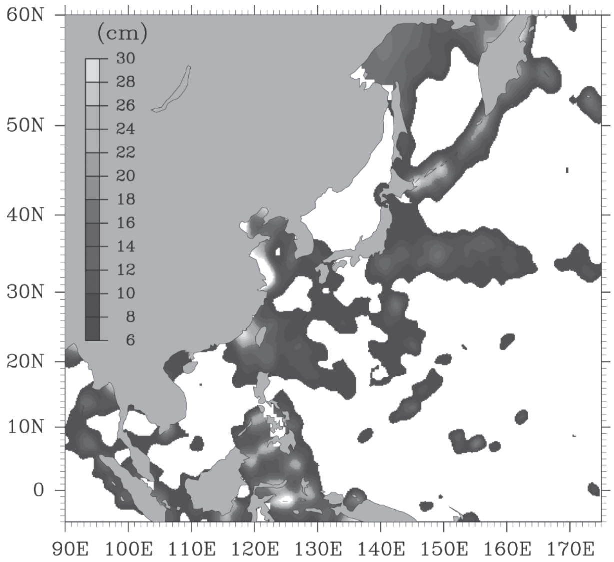

Fig. 1 Sum of the tidal amplitudes of four principal constituents derived from the tidal corrected data set. Only areas with amplitude more than 6 cm are shown.

When the altimetry data are used in the above regions, tidal correction must be applied by harmonic analysis or from the outputs of an accurate tidal model. In the present study, tidal signals were eliminated from AVISO altimetry data using tidal values from NAO 99b, which is the most accurate numerical model for the Asian Marginal Seas, and a new data set is formed.

Kuroshio variations northeast of Taiwan

The region northeast of Taiwan is known to be an active upwelling area with nutrient supply from the Kuroshio subsurface layer. Short- and long-term current variations in relation to the Kuroshio path with a time scale of a few days and a few months on the shelf break northeast of Taiwan have been reported from discontinuous hydrographic or relatively short-term mooring current observations with a low spatio-temporal resolution. However, the temporal-spatial characteristics of the Kuroshio variations northeast of Taiwan and the relation between these Kuroshio variations and the upwelling as well as the onshore transport of subsurface water have not been well addressed. In the present study, analysis of surface current data with a high spatio-temporal resolution, obtained using long-range high-frequency radar (provided by NICT), have clarified the spatio-temporal characteristics of the Kuroshio variations northeast of Taiwan.

The Kuroshio path northeast of Taiwan has long-term variations with periods longer than 30 days and short-term variations with periods of 11–14 days. The Kuroshio variations with periods longer than 30 days are categorized into two types: one is characterized by temporal variation with seasonality, while the other is characterized by the absence of seasonality. In addition, the short-term Kuroshio variations, which are characterized by the biweekly periodic Kuroshio meanders (Fig. 2b-1), are closely related to the appearance of cyclonic eddies propagating from the East Taiwan Channel between Taiwan and Yonagunijima (Fig. 2a). Along with the meanders, an onshore current with large horizontal divergence is formed and crosses the shelf break northeast of Taiwan. The enhanced horizontal divergences associated with this onshore current raise the possibility of topographically controlled upwelling.

These results indicate that the short-term Kuroshio meanders in the East China Sea are caused not only by the local effect of baroclinic instability at the shelf break, but also by the remote effect of downstream propagation of meanders from upstream regions.

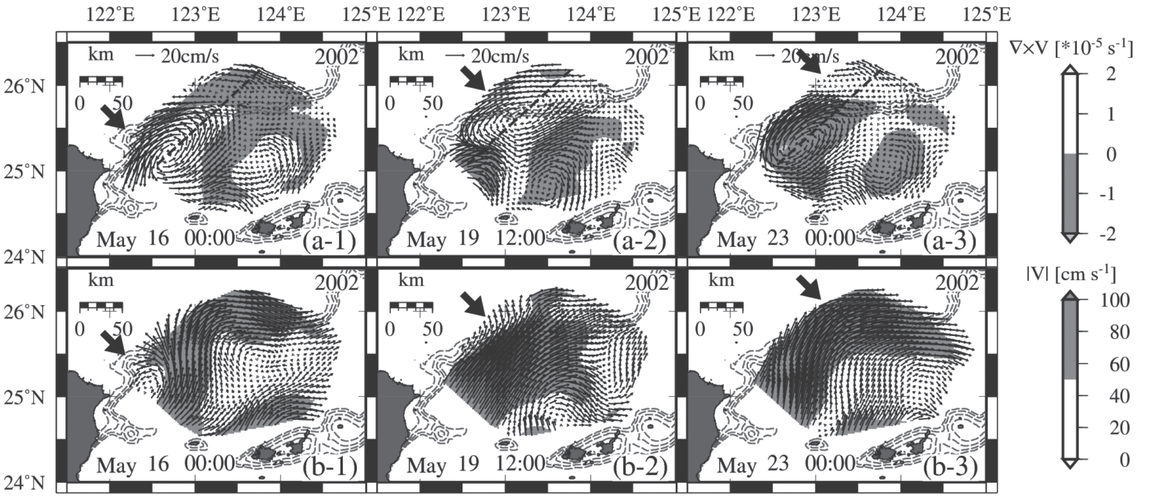

Fig. 2 Horizontal distributions of (a) 11–14 day band-pass-filtered currents and relative vorticity, and (b) low-pass-filtered surface currents during the period between 16 and 23 May 2002. The time interval between panels is 3.5 days. Black arrows indicate cyclonic eddy propagating from the East Taiwan Channel between Taiwan and Yonagunijima.

List of Publications

* : Staffs, students and research fellows in the HyARC.

1. Babiker, I.S., A.A.M. Mohamed and T. Hiyama*
Assessing groundwater quality using GIS. *Water Resources Management*, **21**, 699-715, 2007.
2. Fukutomi, Y., K. Masuda and T. Yasunari*
Cyclonic Activity Associated with the Interannual Seesaw Oscillation of Summer Precipitation over Northern Eurasia. *Global and Planetary Change,* **56**, 387-398, 2007.
3. Fujiki, T. and T. Saino*
Estimation of phytoplankton productivity using chlorophyll fluorescence. *Bulletin on Coastal Oceanography*, Vol.**45**(1), 5-10, 2007.
4. Higuchi, A., T. Hiyama*, Y. Fukuta, R. Suzuki and Y. Fukushima
The behavior of a surface temperature/vegetation index (TVX) matrix derived from 10-day composite AVHRR images over monsoon Asia. *Hydrological Processes*, **21**, 1148-1156, 2007.
5. Hiyama, T.*, M.A. Strunin, H. Tanaka and T. Ohta
The development of local circulations around the Lena River and their effect on tower-observed energy imbalance. *Hydrological Processes*, **21**, 2038-2048, 2007.
6. Ichikawa, H.* and T. Yasunari*
Propagating diurnal disturbances in the Madden-Julian Oscillation. *Geophysical Research Letters*, **34**, L18811, doi: 10.1029/2007GL030480, 2007.
7. Katano, T., A. Kaneda, N. Kanzaki, Y. Obayashi, A. Morimoto*, G. Onitsuka, H. Yasuda, S. Mizutani, Y. Kon, K. Hata, H. Takeoka and S. Nakano
Distribution of prokaryotic picophytoplankton from Seto Inland Sea to the Kuroshio region, with special reference to 'Kyucho' events. *Aquatic Microbialecology*, **46**, 191- 201, 2007.
8. Kobayashi, N.*, T. Hiyama*, Y. Fukushima, M.L. Lopez, T. Hirano and Y. Fujinuma
Nighttime transpiration observed over a larch forest in Hokkaido, Japan. *Water Resources Research*, **43**, W03407 (10.1029/2006WR005556), 2007.
9. Islam, M.N. and H. Uyeda*
Use of TRMM in determining the climatic characteristics of rainfall over Bangladesh. *Remote Sensing of Environment*, **108**(3), 264-276, 2007.
10. Li, Z., T. Takeda, K. Tsuboki*, K. Kato, M. Kawashima and Y. Fujiyoshi
Nocturnal development of cloud clusters during the Meiyu Period in Eastern China. *Journal of the Meteorological Society of Japan*, **85**(1), 25-45, 2007.
11. Li, W.*, T. Hiyama* and N. Kobayashi*
Turbulence spectra in the near-neutral surface layer over the Loess Plateau in China. *Boundary-Layer Meteorology*, **124**, 449-463, 2007.
12. Liu, Y. and T. Hiyama*
Detectability of day-to-day variability in the evaporative flux ratio: A field examination in the Loess Plateau of China. *Water Resources Research*, doi: **10**.1029/2006WR005726, 2007.
13. Masunaga, H.*
Seasonality and Regionality of the Madden-Julian Oscillation, Kelvin Wave, and equatorial Rossby Wave. *Journal of the Atmospheric Sciences*, **64**, 4400-4416, 2007.
14. Moteki, Q., R. Shirooka, K. Yoneyama, B. Geng, M. Katsumata, T. Ushiyama, H. Yamada, K. Yasunaga, N. Sato, H. Kubota, K.K. Reddy, H. Tokinaga, A. Seiki, M. Fujita, Y.N. Takayabu, M. Yoshizaki, H. Uyeda* and T. Chuda
The Impact of the Assimilation of Dropsonde Observations during PALAU2005 in ALERA. *Scientific Online Letters on the Atmosphere (SOLA)*, **3**, 97-100, 2007.
15. Ohigashi, T*. and K. Tsuboki*
Shift and Intensification Processes of the Japan-Sea Polar-Airmass Convergence Zone Associated with the Passage of a Mid-Tropospheric Cold Core. *Journal of the Meteorological Society of Japan*, **85**(5), 633-662, 2007.
16. Patil, S.J., H. Kimoto, T. Kimoto and T. Saino*
Ultraviolet radiation (UV-C): a potential tool for the control of biofouling on marine optical instruments. *Biofouling*, **23**(4), 215-230, 2007.

17. Saino, T.*
A summary of the symposium on "New perspectives of ocean primary productivity research in coastal seas". *Bulletin on Coastal Oceanography*, Vol.**45**(1), 1-3, 2007.
18. Saino, T*
Ocean primary productivity monitoring using an underwater profiling buoy system. *Bulletin on Coastal Oceanography*, Vol.**45**(1), 17-28, 2007.
19. Sukigara, C. and T. Saino*
Monitoring of particle transport from Tokyo Bay to open ocean. *Bulletin on Coastal Oceanography*, Vol.**45**(1), 51-59, 2007.
20. Sarma, V.V.S.S., M. Dileep Kumar and T. Saino*
Impact of sinking carbon flux on accumulation of deep-ocean carbon in the Northern Indian Ocean. *Biogeochemistry*, **82**(1), 89-100, DOI 10.1007/s10533-006-9055-1, 2007.
21. Sasai, T., K. Okamoto, T. Hiyama* and Y. Yamaguchi
Comparing terrestrial carbon fluxes from the scale of a flux tower to the global scale. *Ecological Modelling*, **208**, 135-144, 2007.
22. Suzuki, S., K. Shiokawa, Y. Otsuka, T. Ogawa, K. Nakamura* and T. Nakamura
A concentric gravity wave structure in the mesospheric airglow images. *Journal of Geophysical Research*, **112**, D02102, doi: 10.1029/2005JD006558, 2007.
23. Tanaka, H., T. Hiyama*, K. Yamamoto, H. Fujinami*, T. Shinoda*, A. Higuchi, S. Endo*, S. Ikeda, W. Li and K. Nakamura*
Surface flux and atmospheric boundary layer observations from the LAPS project over the middle stream of the Huaihe River basin in China. *Hydrological Processes*, **21**, 1997-2008, 2007.
24. Takahashi, D.*, K. Kido, Y. Nishida, N. Kobayashi, N. Higaki, H. Miyake
Dynamical structure and wind-driven upwelling in a summertime anticyclonic eddy within Funka Bay, Hokkaido, Japan. *Continental Shelf Research*, **27**, 1928-1046, 2007.
25. Yamada, H., B. Geng, H. Uyeda* and K. Tsuboki*
Thermodynamic Impact of the Heated Landmass on the Nocturnal Evolution of a Cloud Cluster over a Meiyu-Baiu Front. *Journal of the Meteorological Society of Japan*, **85**(5), 663-685, 2007.
26. Yamada, H., B. Geng, H. Uyeda* and K. Tsuboki*
Role of the Heated Landmass on the Evolution and Duration of a Heavy Rain Episode over a Meiyu-Baiu Frontal Zone. *Journal of the Meteorological Society of Japan*, **85**(5), 687-709, 2007.
27. Yasunari, T.*
Role of Land Atmosphere Interaction on Asian Monsoon Climate. *Meteorological Society of Japan*, **85B**, 55-75, 2007.

Hydrospheric Atmospheric Research Center (HyARC)
Nagoya University

Furo-cho, Chikusa-ku, Nagoya 464-8601, Japan

Office:

Telephone: +81-52-789-3466
Facsimile: +81-52-789-3436
Home Page: http://www.hyarc.nagoya-u.ac.jp/hyarc/

The 2007 Annual Report was published July 2008 by the Hydrospheric Atmospheric Research Center (HyARC) Nagoya University. Copies of this report are available from the office of the Center.

Printed by Nagoya University COOP


HyARC
Hydrospheric Atmospheric Research Center, Nagoya University